https://doi.org/10.5194/egusphere-2025-830
Preprint. Discussion started: 26 February 2025

Observations of tropospheric HONO are incompatible with understanding of atmospheric chemistry

Matthew J. Rowlinson[1,2], Lucy J. Carpenter[1], Mat J. Evans[1], James D. Lee[1,2], Simone T. Andersen[3], Tomas Sherwen[4], Anna B. Callaghan[1], Roberto Sommariva[5], William Bloss[5], Siqi Hou[5], Leigh R. Crilley[6], Klaus Pfeilsticker[7], Benjamin Weyland[7], Thomas B. Ryerson[8], Patrick R. Veres[9,⊥], Pedro Campuzano-Jost[11], Hongyu Guo[13], Benjamin A. Nault[12,13] and Jose L. Jimenez [10,11], Khanneh Wadinga Fomba[14]

[1] Wolfson Atmospheric Chemistry Laboratories, Department of Chemistry, University of York, York, YO10 5DD, UK
[2] National Centre for Atmospheric Science, University of York, York, YO10 5DD, UK
[3] Atmospheric Chemistry Department, Max Planck Institute for Chemistry, 55128 Mainz, Germany
[4] Hephaestus Partners, Ealing, London, UK, W7
[5] School of Geography Earth and Environmental Sciences, University of Birmingham, Birmingham, B15 2TT, UK
[6] Atmospheric Services, WSP Australia, Brisbane, Australia
[7] Institute of Environmental Physics, University of Heidelberg, Heidelberg, Germany
[8] National Oceanic and Atmospheric Administration (NOAA), Chemical Sciences Laboratory (CSL), Boulder, CO, USA
[9] Chemical Sciences Division, Earth System Research Laboratory, National Oceanic and Atmospheric Administration, Boulder,
O, USA
[10] NASA Langley Research Center, Hampton, VA, USA
[11] Cooperative Institute for Research in Environmental Sciences and Department of Chemistry, University of Colorado Boulder,
Boulder, CO, USA
[12] Center for Aerosol and Cloud Chemistry, Aerodyne Research Inc., Billerica, MA, USA
[13] Department of Environmental Health and Engineering, Johns Hopkins University, Baltimore, MD, USA
[14] TROPOS – Leibniz-Institute for Tropospheric Research, Permoserstr. 15, 04318 Leipzig, Germany
[⊥] Now at National Science Foundation National Center for Atmospheric Research, Boulder, Colorado, USA

Correspondence: Matthew J. Rowlinson (matthew.rowlinson@york.ac.uk)
Mat J. Evans (mat.evans@york.ac.uk)

Abstract. Recent observations of nitrous acid (HONO) in the remote troposphere found much higher concentrations than can be explained through known sources, with important implications for air quality and climate. Laboratory evidence and modelling of field observations suggests that nitrate aerosol photolysis is the likely mechanism providing the additional HONO, offering a rapid route for recycling of NO_x from nitric acid (HNO_3). Previous studies of the global impact of this chemistry have used either very restricted HONO data or a "top-down" approach to parameterize the HONO source by reconciling simulated and observed NO_x concentrations. Here, we use multiple, independent tropospheric HONO observations from different locations to parameterize nitrate photolysis, and evaluate its impacts on global atmospheric chemistry using GEOS-Chem. The simulations improve agreement between modelled and observed HONO concentrations relative to previous studies, decreasing the model bias by 5-20%. The remaining (and large) underestimate of HONO in the model is due predominantly to an underestimate of total nitrate aerosol (-95%) and is reduced to 20% when accounting for low model nitrate. Despite the low bias in the model HONO, we find that nitrate aerosol photolysis leads to substantial global increases in NO_x, O_3 and OH concentrations, likely beyond the observational constraints. The additional source of NO_x (~48 Tg N yr^{-1} globally) is comparable to total NO_x emissions from all sources (~55 Tg yr^{-1}). These HONO

https://doi.org/10.5194/egusphere-2025-830
Preprint. Discussion started: 26 February 2025

observations in the remote troposphere, thus imply a large uncertainty in the NO_x budget and an incomplete understanding of atmospheric chemistry.

1 Introduction

Nitrogen oxides (NO_x: NO + NO_2) and hydroxyl radicals (OH) are crucial drivers and regulators of atmospheric chemistry processes (Monks et al., 2015; Nguyen et al., 2022). NO_x catalyses the production of ozone (O_3), a significant air pollutant (Monks et al., 2015) and greenhouse gas (Szopa et al., 2021) and modulates the abundance and distribution of OH. OH is known as the atmosphere's "self-cleansing agent" and is the primary oxidant of hydrocarbons, leading to O_3 formation and the production of particulate nitrate aerosol (NO_3^-), a significant contributor to the atmospheric aerosol load and its radiative effects. Nitrous acid (HONO) is a key species in the cycling between NO_x and HO_x (OH + HO_2) radicals and therefore is also central to regulating tropospheric O_3 (Jiang et al., 2023). NO_x is removed from the atmosphere predominantly by the reaction of OH with NO_2 to give nitric acid (HNO_3) or through the hydrolysis of dinitrogen pentoxide (N_2O_5) on aerosol surfaces to give particulate nitrate (pNO_3^-) (Ramazan et al., 2006; Stavrakou et al, 2013). There is rapid cycling between the gas (HNO_3) and particulate phase nitrate. HNO_3 and pNO_3^- are soluble and removed rapidly through wet and dry deposition (Parrish et al., 1986; Meng et al., 1997). HNO_3 can return reactive nitrogen compounds through photolysis or reaction with OH, but these reactions are slow relative to deposition. Conversion of reactive nitrogen oxides to HNO_3 or pNO_3^- has traditionally therefore been considered a terminal sink for reactive nitrogen oxides (Knipping and Dabdub, 2002).

There is however a growing body of laboratory and field evidence that pNO_3^- can be rapidly photolysed to produce HONO and NO_2 (with yields x and y; R1) (Ndour et al., 2009; Ye et al., 2016; Ninneman et al., 2020; Shi et al., 2021).

$$pNO_3^- + h\nu \rightarrow xHONO + yNO_2 \qquad J_{pNO_3^-} \ (R1)$$

This return of reactive nitrogen compounds from HNO_3 and pNO_3^- has been termed "renoxification" (Lary et al., 1997; Bekki et al., 1997; Ndour et al., 2009), effectively acting as a secondary chemical source of NO_x. Laboratory studies have found that R1 occurs 10-1700 times faster than HNO_3 photolysis under atmospheric conditions, typically expressing this rate as an enhancement factor (EF) relative to the rate of HNO_3 photolysis (EF = J_{pNO3-} / J_{HNO3}) (Ye et al., 2016; Ye et al., 2017; Bao et al., 2018; Shi et al., 2021; Sommariva et al., 2023).

Recent field studies have demonstrated that renoxification is a plausible mechanism for the production of HONO measured in the remote oceanic atmosphere (Ye et al., 2016; Reed et al., 2017; Bao et al., 2018; Zhu et al., 2022; Andersen et al., 2023). In such environments, where NO_x concentrations are low, HONO is typically thought to be produced slowly from the gas phase reaction of OH with NO. While there are various alternative direct or chemical sources of HONO in polluted air (Yu et al., 2022; Song et al., 2023), these are expected to be very slow in clean, background air (Andersen et al., 2023). Crilley et al. (2021) further showed that any oceanic direct emission source is also negligible. HONO is lost rapidly by photolysis, hence concentrations are expected to be low in the marine atmosphere (generally mixing ratios < 1 pptv; Reed et al., 2017). However, HONO measurements have revealed atmospheric concentrations significantly higher than would be expected from this gas phase chemistry alone (Ye et al., 2016; Reed et al., 2017; Ye et al., 2017; Zhu et al., 2022; Andersen et al., 2023; Ye et al., 2023; Zhong et al., 2023; Weyland et al., 2024), challenging our understanding of atmospheric chemistry. This renoxification process could represent an important source of NO_x in remote or marine regions where there are few other reactive nitrogen sources (Kasibhatla et al., 2018; Shah et al., 2023).

Tropospheric O_3 is formed in the atmosphere when carbon monoxide, methane or volatile organic compounds (VOCs) are oxidized in the presence of NO_X. In remote regions far from human activity, low emissions mean that NO_x is generally the limiting factor for O_3 production, therefore a secondary *in-situ* source of NO_x from nitrate photolysis could have important implications for background concentrations of tropospheric O_3. Long term measurements show that background tropospheric

https://doi.org/10.5194/egusphere-2025-830
Preprint. Discussion started: 26 February 2025

O_3 levels have been increasing in recent decades (Gaudel et al., 2018). Shah et al. (2024) showed that nitrate photolysis could partially explain the observed trend. With decreasing SO_2 emissions and increasing ammonia emissions leading to decreased aerosol acidity (Bauer et al., 2007; Bauer et al., 2020), nitrate aerosol concentrations have increased (Bauer et al., 2020). If this trend were to continue, nitrate photolysis could drive a continued increase in background tropospheric O_3 concentrations.

A number of studies have implemented pNO_3^- photolysis into chemical transport models. Kasibhatla et al. (2018) found that implementing nitrate photolysis on sea-salt aerosols with EFs of 25-50 improved model simulation of marine NO_x concentrations. However, EFs of 100 were required to adequately simulate HONO measurements in the remote marine boundary layer, resulting in an overestimate of NO_x relative to observations. Shah et al. (2023) successfully reproduced NO observations in the free troposphere when applying an EF of 100, scaled to the sea-salt:nitrate aerosol ratio, but did not evaluate the model's ability to reproduce HONO observations. Similarly Dang et al. (2023) used the same nitrate photolysis parameterization and again found significant improvement in the modeling of NO_2. These parameterizations were not based directly on the observed mechanism but rather by reverse-engineering the process to produce the expected NO_x and O_3 concentrations. Thus, knowledge of the precise impact of nitrate photolysis as seen in laboratory and field studies and the effect of measured HONO is currently unknown.

Here we use recent measurements of HONO made in remote locations (Section 2.1), together with the GEOS-Chem chemistry transport model (Section 2.2) to develop a new parameterization of the EF (Section 3) and implement it into the model. We then assess its impact on HONO concentrations in the model (Section 4) and the impact of nitrate photolysis on the composition of the troposphere (Section 5). The wider impacts of this process on our understanding of atmospheric chemistry are then discussed in Section 6.

2 Methods

Here we describe the datasets and tool used for the analysis. We first describe field observations of the concentration of HONO and other species and then the configuration of the GEOS-Chem model.

2.1 Field Measurements

2.1.1 ARNA Campaign

The ARNA (Atmospheric Reactive Nitrogen over the remote Atlantic) field campaigns took place over the tropical Atlantic Ocean in August 2019 and February 2020 using the FAAM BAe-146-301 atmospheric research aircraft and in August 2019 at the Cabo Verde Atmospheric Observatory (CVAO; Figure S1). Twelve flights (four in summer and eight in winter) were conducted with in situ measurements including NO, NO_2, HONO, O_3, and aerosol surface area. pNO_3- was determined from aerosol filters sampled over each straight-and-level run. HONO concentrations were determined using differential photolysis as described in Andersen et al. (2023). This technique photolytically converts both NO_2 and HONO into NO. Subsequently, NO is detected using chemiluminescence with a dual-channel instrument featuring two custom-built photolytic converters. HONO conversion efficiencies were calibrated against measurements from ultraviolet-visible cavity enhanced absorption spectroscopy conducted at HIRAC (The Highly Instrumented Reactor for Atmospheric Chemistry), following the methodology of Reed et al. (2016). The average detection limit for HONO across the study period was 4.2 pptv at the 2-sigma level. At the CVAO, NO_x, pNO_3-, O_3, and photolysis rates are measured routinely (Carpenter et al., 2010) and these were supplemented by HONO measurements described in Section 2.1.5

2.1.2 FIREX-AQ

The FIREX-AQ campaign was conducted from July to September 2019, with multiple aircraft deployed from California, Idaho and Kansas in the USA (Bourgeois et al., 2022; Warneke et al., 2022). The datasets were collected from an archived

https://doi.org/10.5194/egusphere-2025-830
Preprint. Discussion started: 26 February 2025

merged dataset (https://www-air.larc.nasa.gov/cgi-bin/ArcView/firexaq), averaged over 60 second intervals. In order to get measurements representative of 'clean' or background air, measurements are excluded when the concurrent CO concentration exceeds 120 ppb, which would be indicative of pollution from either a biomass burning or anthropogenic source.

HONO was measured using an iodine-adduct chemical ionization mass spectrometer (CIMS) (Lee et al., 2014; Veres et al., 2020; Bourgeois et al., 2022). Ambient air mixed with reagent ions, specifically iodide ions and iodide-water clusters, was ionized and analyzed for mass-to-charge ratio. HONO was detected as a cluster with iodide, and background signals were accounted for to determine ambient HONO levels. The fixed-temperature measurement uncertainty is ±(15% + 3 pptv), with a precision of ±2 pptv for 1 s data.

NO_x was measured with ozone induced chemiluminescence, with three channels measuring NO, NO_2 and NO_y, respectively. The instrument continuously samples ambient air from an aircraft, with specific flow rates for each gas. Instrument calibrations occur both on the ground and in-flight, and measurements are taken with high temporal resolution. Corrections are applied for factors like water vapor content and interference from other compounds. The estimated measurement uncertainties at 1hz for NO, NO_2, and NO_y at sea level are ±(4% + 6 pptv), ±(7% + 20 pptv), and ±(12% + 15 pptv), respectively.

Carbon monoxide (CO) was measured by tunable diode laser absorption spectroscopy (TDLAS) using the DACOM (Differential Absorption Carbon monoxide Measurement) instrument (Sachse et al., 1987; Sachse et al., 1991; Bourgeois et al., 2022). TDLAS used three single-mode tunable diode lasers, measuring CO using a quantum cascade laser (QCL) at 4.7 μm. Measurement precision (1σ), calculated after the campaign, was approximately 0.1% at 1 s.

Bulk nitrate aerosol measurements used to produce the nitrate photolysis parameterization (Figure 2) were made with the Soluble Acidic Gases and Aerosol (SAGA) filter collector with subsequent offline IC analysis (Dibb et al., 1999; Dibb et al., 2002; Scheuer et al., 2003). Sample resolution during FIREX-AQ was 2-5 minutes. Concentrations of chloride and other ions were also reported. SAGA has a detection limit of 1 to 25 pptv depending on the sampled species.

A high-resolution aerosol mass spectrometer (HR-AMS) was used to measure fine-mode particulate nitrate (pNO_3^-) at a high time resolution (Guo et al., 2021; Bourgeois et al., 2022). Submicron aerosol composition was derived using flash vaporization of the aerosol, followed by 70 eV electron ionization of the volatilized gas phase and analysis by mass spectrometry. Typical detection limits were ~30 ppt.

2.1.3 CAFÉ-Africa

The Chemistry of the Atmosphere: Field Experiment in Africa (CAFE-Africa) campaign took place in August and September 2018, with 14 flights from Cabo Verde over the Atlantic Ocean and West African coastline. A 'mini-DOAS' was deployed on the German High-Altitude and Long-Range (HALO) research aircraft to measure HONO. The mini-DOAS is an airborne six-channel optical spectrometer, which records UV, visible, and near infra-red light in the nadir and limb viewing geometries. The spectrometers are kept in an evacuated and cooled housing in the otherwise unpressured, uninsulated fuselage of the HALO aircraft. Collected skylight spectra are analyzed for signatures of light absorption by trace gases using the DOAS technique. Slant column densities of trace gases determined by the DOAS technique are then converted to volume mixing ratios or concentrations by the novel scaling method. The scaling method requires a gas whose concentration is known or otherwise measured in situ, to construct a proportional relationship between concentrations and slant column densities. The Monte Carlo radiative transfer model McArtim helps to attribute absorption to specific layers of the atmosphere. Gas concentrations retrieved with the scaling method represent averages over several dozen square kilometers as a function of the mean light path length, as well as the distance traveled by the aircraft during integration of the spectra. Due to the dependence on pathlength and large variations with altitude and visibility, no reliable, overall limit of detection has been established for this technique.

2.1.4 SEANA

The Shipping Emissions in the Arctic and North Atlantic atmosphere (SEANA) project took place between 20 May and 26 June 2022 around the coast of Greenland (Zhang et al., 2024). HONO was measured using a Long Path Absorption Photometer (LOPAP-03, Quma GmbH) during the DY151 cruise aboard the RSS Discovery research ship. HONO was sampled within a

https://doi.org/10.5194/egusphere-2025-830
Preprint. Discussion started: 26 February 2025

stripping coil into an acidic solution and derivatized with an azo dye. Absorption of light (550 nm) by the azo dye was measured with an Ocean Optics spectrometer using an optical path length of 2.4 meters. The technique is described in detail in Heland et al., 2001. The instrument was calibrated and operated following the standard operating procedures described in Kleffman and Wiesen 2008.
The LOPAP instrument was located inside a shipping container on the foredeck of the ship and was sampling via a 3 meters long umbilical to the inlet located on the roof of the shipping container. The detection limit of the LOPAP during the cruise was between 0.7 and 1.5 ppt (2-sigma, 30 seconds), with an estimated relative error of 10%.
A zero signal was taken at regular intervals (6 hours) by overflowing the inlet with dry nitrogen for 30 minutes. The zero signals were linearly interpolated to obtain a baseline which was then subtracted from the calibrated signal. Because of the very low HONO levels in the Arctic Ocean, the LOPAP signal was sometimes indistinguishable from the zero signal. A correction factor of 1.5-3.5 ppt was therefore applied to the final time series on the assumption that the HONO concentration in the darkest period of the Arctic day is zero. Due to the inherent uncertainties in this assumption the reported values should be considered lower limits.

2.1.5 Cabo Verde Atmospheric Observatory

The Cabo Verde Atmospheric Observatory (CVAO) is a World Meteorological Organisation (WMO) Global Atmospheric Watch (GAW) site that operates on the north-west coast of São Vincente, Cabo Verde (16°51' N, 24°52' W). Measurements at the site are considered to be representative of clean, marine background air (Carpenter et al., 2010).

HONO has been measured at the CVAO in November-December 2015 (Reed et al., 2017), August 2019, February 2020 (Andersen et al., 2023) and in February 2023, using a long-path absorption photometer (LOPAP-03 QUMA Elektronik & Analytik GmbH). A full description of the instrument's operating principle and measurement technique can be found in Heland et al. (2001) and Kleffman et al. (2007). In the 2023 campaign, the inlet for the LOPAP was placed on top of a shipping container (roughly 3 m agl). Zeroes were measured every 6 hours for 30 minutes using an N5 N_2 cylinder. The instrument was calibrated using a Titrisol nitrite standard solution (1000 mg of NO_2^- diluted to 0.01 mg L^{-1}) on 9th, 11th and 21st February. The detection limit was 0.3 ppt (2s), calculated using the noise during zero measurements. As recommended by QUMA, the relative error of the instrument was set at 10% of the measured HONO value. Particulate nitrate (pNO_3^-) was measured in 24-hour samples using a PM10-inlet and subsequent laboratory analysis using standard ion chromatography technique (Fomba et al., 2014).

2.1.6 Tudor Hill Observatory

The Tudor Hill Marine Atmospheric Observatory is a continuous monitoring station located on the island of Bermuda (32°15' N, 64°52' W). In field studies in 2019, ambient HONO concentrations were measured continuously by a long-path absorption photometry (LOPAP) system (Zhu et al., 2022). Corrections were done using the zero-HONO air generated by pulling ambient air through the Na_2CO_3 denuder. The LOPAP system, described in detail in Zhu et al., (2022), has been widely used and proven accurate in HONO measurement during the previous NOMADSS field campaigns (Ye et al., 2016, Ye et al., 2018). The detection limit was calculated as ~0.6 pptv at 10 min time resolution. Ambient HNO_3 and pNO_3^- were also measured by similar LOPAP systems, where the nitrate was converted into nitrite through a Cd column in NH_4Cl buffer solution. The detection limit of particulate nitrate measured by the LOPAP system was ~17 pptv (3σ) at 10 min time resolution. NO_x concentrations were measured by a low-level commercial chemiluminescence analyzer.

2.1.7 ATom

The NASA Atmospheric Tomography mission (ATom) consisted of four aircraft campaigns conducted between August 2016 and May 2018 (Wofsy et al., 2021; Thompson et al., 2022). Using NASA DC-8 research aircraft, ATom provided detailed datasets of atmospheric composition with an extensive spatial coverage, in particular over oceans. Here used the 10-second merged ATom dataset for all four seasonal campaigns (https://doi.org/10.3334/ORNLDAAC/1925) (Wolfsy et al., 2021). The data was filtered to only use data measured over the ocean, to broadly avoid polluted air.

https://doi.org/10.5194/egusphere-2025-830
Preprint. Discussion started: 26 February 2025

2.2 GEOS-Chem

The three simulations were completed using the 3-D global chemical transport model GEOS-Chem, version 14.2.2 (Bey et al., 2001) (http://www.geos-chem.org, last access: 31 March 2024; https://zenodo.org/records/10034814, The International GEOS-Chem User Community, 2022). The model was driven by MERRA-2 meteorology from the NASA Global Modeling and Assimilation Office (Gelaro et al., 2017), with 72 vertical levels and a spatial resolution of 4.0° × 5.0°. All simulations were run for 2 years through 2018 and 2019, with the first year considered spin-up. The model used an updated chemical mechanism with improved benzene, toluene and xylene oxidation chemistry, as described by Bates et al. (2021). The model used biomass burning emissions from GFED4s (van der Werf et al., 2017) and biogenic emissions from MEGAN v2.1 (Guenther et al., 1995). Anthropogenic emissions are from the Community Emissions Data System (CEDS) (Hoesly et al., 2018; McDuffie et al., 2020).
The Shah parameterization for nitrate photolysis was developed by Shah et al. (2023) and is incorporated into the standard GEOS-Chem model. They found best agreement with NO observation with an EF of 100 applied to coarse-mode nitrate, while the EF for fine-mode nitrate was scaled based on the pNO_3^- to sea-salt ratio. For the purposes of this study, nitrate photolysis according to Shah et al. (2023) was switched off in the model for the "Base" simulation and turned on in the "Shah" simulation.

When simulating the preindustrial atmosphere, anthropogenic emissions for the year 1750 are taken from CEDS (Hoesly et al., 2018), with natural emissions matching the present-day simulations and meteorology for the year 2019. Methane (CH_4) for the year 1750 is prescribed from the CMIP6 dataset (Meinshausen et al., 2017). A normalised radiative forcing (NRF) of 42 mW m^{-2} DU^{-1} (Stevenson et al., 2013) is used to calculate the preindustrial to present-day O_3 radiative forcing.
Normalized mean bias is used to assess model performance compared to observations, defined here as $NMB = \sum_{i=1}^{n}(P_i - O_i) / \sum_{i=1}^{n} O_i$, where P are the simulated values and O is the observations. The nitrate photolysis parameterisation was developed by fitting a non-linear least squares function to the observed data, using the SciPy python package (https://docs.scipy.org/doc/scipy-1.15.0/reference/generated/scipy.optimize.curve_fit.html; Virtanen et al., 2020).

3 Development of a nitrate aerosol photolysis parameterization

Here we use observations of HONO, nitrate aerosol and photolysis rates from (1) the Atmospheric Reactive Nitrogen over the remote Atlantic (ARNA) aircraft campaign over the Tropical Atlantic (Andersen et al., 2023), (2) the Fire Influence on Regional to Global Environments Experiment - Air Quality (FIREX-AQ) aircraft campaign over the continental USA (Warneke et al., 2023) and (3) HONO measurements from the Cabo Verde Atmospheric Observatory (see Methods Section), to generate a parameterization of the nitrate aerosol photolysis process. This is then applied in GEOS-Chem to simulate HONO concentrations and evaluated with independent HONO measurements from the Chemistry of the Atmosphere: Field Experiment in Africa (CAFE-Africa) aircraft campaign in the Atlantic (Weyland et al., 2024), the Shipping Emissions in the Arctic and North Atlantic Atmosphere (SEANA) ship campaign and from Tudor Hill, Bermuda (Zhu et al., 2022). The locations and measured concentrations of HONO in the various campaigns are shown in Figure S1.

Following Ye et al. (2016), we assume that the photolysis of nitrate aerosol leads to the production of 0.66 HONO molecules and 0.33 NO_2 molecules (R1). The photolysis of HONO is its dominant sink (R2) with a lifetime in the tropical marine boundary layer of about 12 minutes (Ye et al., 2016; Andersen et al., 2023) and thus we derive a rate equation by placing HONO into steady state (Equation 1 and 2).

$$HONO + h\nu \rightarrow OH + NO \qquad J_{HONO}\ (R2)$$

Thus;

https://doi.org/10.5194/egusphere-2025-830
Preprint. Discussion started: 26 February 2025

$$\frac{d[HONO]}{dt} = \frac{2}{3} \times J_{NO_3^-} \times [pNO_3^-] - J_{JONO} \times HONO \quad (1)$$

$$[HONO] = \frac{2}{3} \times \frac{J_{NO_3^-}}{J_{HONO}} \times [pNO_3^-] \quad (2)$$

Where J_{HONO} and J_{NO3-} refer to the rate of photolysis of HONO and pNO_3^-, respectively. Following Ye et al., 2016 we assume that the photolysis of nitrate is equal to the photolysis rate for gas phase HNO_3 (J_{HNO3}) multiplied by an enhancement factor (EF) which can be rearranged to give Equation 3.

$$EF = \frac{3}{2} \times \frac{[HONO]}{[NO_3^-]} \times \frac{J_{HONO}}{J_{HNO_3}} \quad (3)$$

The renoxification process is thought to be efficiently driven by photolysis of surface-bound rather than bulk nitrate or nitric acid, due to enhanced absorption cross sections and higher quantum yields at the interface compared to bulk solution (Zhu et al., 2010; Du and Zhu 2011; Ye et al., 2017). Further, the presence of certain cations has been shown to lead to preferential distributions of nitrate ion at the interface (Wingen et al., 2008; Richards et al., 2012; Hua et al., 2014). Therefore, following Andersen et al. (2023), we fit a nonlinear function to the observed EF (see Methods Section), derived from the measurements of HONO, nitrate aerosol, J_{HNO3} and J_{HONO} from the CVAO, ARNA and FIREX-AQ campaigns, to a Langmuir isotherm model (Equation 4, Figure 1.).

$$EF = \frac{5.02 \times 10^8}{(1 + 7.19 \times 10^5 \times [pNO_3^-])} \quad (4)$$

We note though that unlike the fit in Andersen et al. (2023), the equation (4) no longer resembles a Langmuir isotherm as the nitrate-dependent portion of the denominator under realistic atmospheric conditions is significantly larger than 1. This may reflect the mixed contribution of surface and bulk processes, the different aerosol compositions in the field campaigns (see discussion below), or other factors.

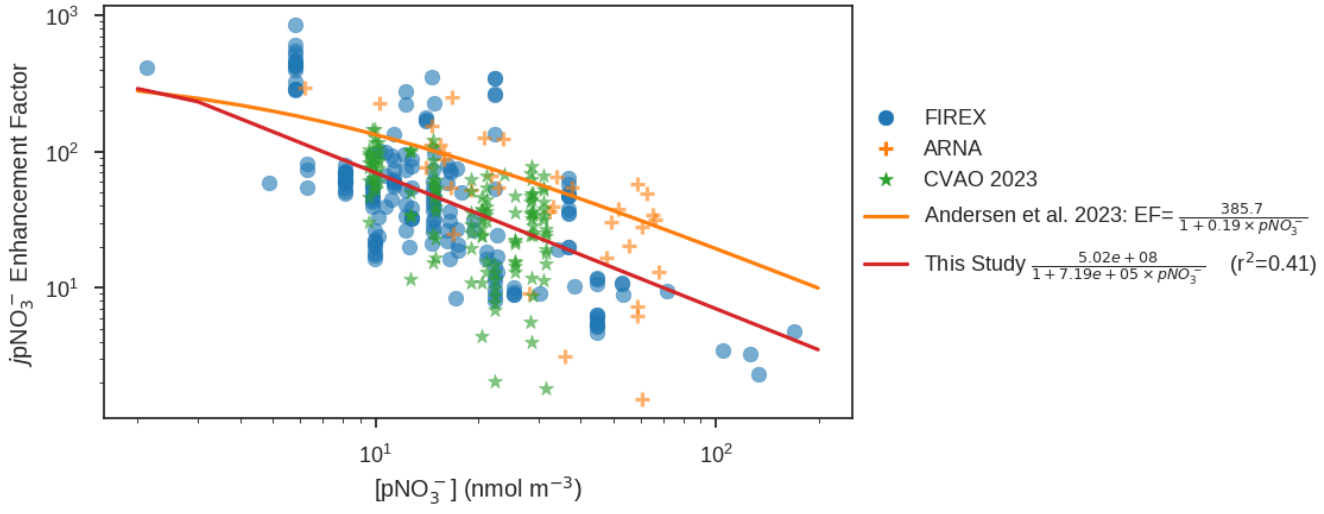

Figure 1. Nitrate aerosol photolysis enhancement factor necessary to balance the observed HONO against its photolytic loss as a function of the nitrate aerosol concentration (see Methods Section).

https://doi.org/10.5194/egusphere-2025-830
Preprint. Discussion started: 26 February 2025

The large range in the estimated EFs from measurements (Figure 1) results in large variance around the fit, with an R-squared value of 0.41. This is not surprising since the measurements span a variety of environments, likely experiencing different aerosol pH, composition and ambient humidity, all of which are known to impact the efficiency of renoxification (Ndour et al., 2009; Gen et al., 2022; Andersen et al., 2023; Sommariva et al., 2023; Li et al., 2024; Jiang et al., 2024). However, more complex parameterizations accounting for such dependencies resulted in only minor improvements in the agreement with observed EFs (see examples in Figure S2 in the supplementary material). Therefore, for the sake of simplicity and due to the paucity of observations, the parameterization with only pNO_3^- dependency was used here.

The mean EF values calculated from the combined ARNA, FIREX-AQ and CVAO measurements are 2-3 times lower than that found in Andersen et al. (2023) using the ARNA campaign alone. This may reflect that the FIREX-AQ observations were over a continental region whereas the Andersen data was collected over the ocean, where sea salt aerosol dominates the aerosol mass. Sodium and chloride ions have been observed to enhance the yield of HONO and NO_2 from particulate nitrate photolysis, attributed to the existence of a double layer of interfacial Cl^- and subsurface Na^+ drawing nitrate ions closer to the interface when the Cl^-:NO_3^- ratio increases (Wingen et al., 2008; Sommariva et al., 2023). The observed bulk chlorine from filter measurements during the ARNA campaign was substantially higher than during FIREX-AQ (median value of 0.63 μg m^{-3} compared to 0.03 μg m^{-3}), reflecting the contrast between marine and terrestrial campaigns and possibly contributing to the difference in calculated EF.

Our parameterization produces a much greater range of EF values (from 3 to 562) than used in previous nitrate photolysis modeling studies (Kasibhatla et al., 2018; Shah et al., 2023). Kasibhatla et al. (2018) used fixed EF values (of between 25 - 100) on sea-salt aerosol and Shah et al., (2023) tied the EF magnitude to the availability of sea-salt with fixed upper and lower EFs, resulting in a range of 10 to 100. While these studies demonstrated that nitrate photolysis could improve model performance in simulating NO_x and O_3, the resulting parameterizations were not based on the EF values derived in laboratory and field studies (Ye et al., 2016; Shi et al., 2021).

4 Evaluation of parameterisation

Here we implement the parameterization of the enhancement factor (Equation 1) into the GEOS-Chem model (see Methods Section and Equation 4). We evaluate this model simulation together with a version with no nitrate photolysis (Base) and that using the Shah et al. (2023) parameterization (Shah) against a wider set of pNO_3^- (Prospero et al., 2001) and HONO observations (CAFE-Africa, SEANA, Tudor Hill). We use a normalized mean bias (NMB; see Methods Section) metric to assess model performance and impact of changes between simulations.

The extent and impact of the simulated nitrate photolysis relies critically on the model's ability to replicate nitrate aerosol. Nitrate aerosol in GEOS-Chem is split into two modes; a fine-mode associated with sulfate and ammonia and a coarse-mode (0.5-8.0 μm) associated with sea-salt and desert dust. Various studies have reported a persistent high-bias in fine-mode nitrate aerosol in GEOS-Chem compared to aerosol mass spectrometry (AMS) observations (Walker et al., 2012; Miao et al., 2020; Zhai et al., 2021a; 2021b; Gao et al., 2022). This may be linked to the model underestimating acidity in remote regions (Nault et al., 2021). There has been little work evaluating the coarse-mode nitrate. Consistent with previous studies, we find that the base simulation without nitrate photolysis significantly overestimates fine-mode nitrate when compared with observations from the NASA Atmospheric Tomography Mission (ATom) campaign (Figure 6a, NMB=+271%) and in some regions of the mid and upper troposphere in the FIREX-AQ campaign (Figure S3), except over California where nitrate is very low, likely due to an underestimate of ammonia emissions (Walker et al., 2012). The inclusion of the nitrate photolysis parameterization generally decreases fine nitrate aerosol concentrations and improves the NMB relative to observations for the ATom campaign from +271% to +93% (Figure 6a).

https://doi.org/10.5194/egusphere-2025-830
Preprint. Discussion started: 26 February 2025

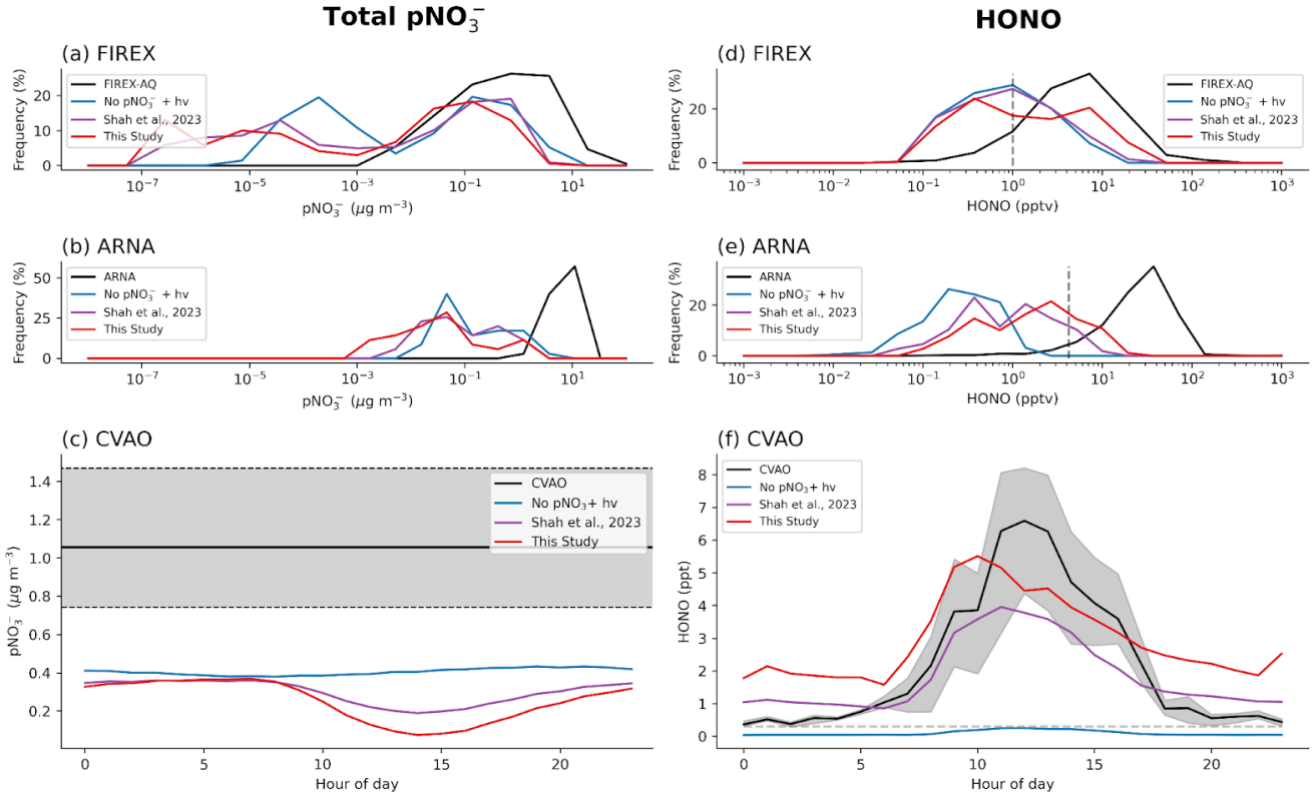

Figure 2. Frequency density comparisons between observed (black) and simulated (Base simulation (blue); Shah simulation (purple); New parameterization (red)) total pNO_3^- (left) and HONO (right) concentrations during the FIREX-AQ campaign (top) and the ARNA campaign (middle). Bottom panels show simulated diurnal concentrations over the Cabo Verde Atmospheric Observatory (CVAO) compared to available observations (HONO diurnal averaged from campaigns in 2015, 2019 and 2023 represented by the black line, grey shading indicating 10th-90th percentile in panel c, 25th-75th percentile in panel f). Dashed grey lines in panels d, e and f represent the estimated limit of detection.

In contrast, total particulate nitrate (Figure 2a-c) observations from FIREX-AQ, ARNA, and CVAO of total nitrate underestimated by the base model with a NMB of -88 to -95%. The inclusion of nitrate photolysis has only a small impact, decreasing aerosol concentrations and resulting in a NMB of between -92 and -98% across the 3 datasets. A further comparison with global surface observations collected between 1980 and the present (Figure 3) (Prospero et al., 2001), also shows the model underestimates total nitrate at the majority of sites. This is likely to be of larger importance in regions with a higher ratio of coarse to fine mode aerosol, such as marine regions where coarse sea-salt aerosol is prominent. Overall, we conclude, consistent with previous studies (Walker et al., 2012; Miao et al., 2020; Zhai et al., 2021a, 2021b; Gao et al., 2022), that the model overestimates fine mode nitrate and significantly underestimates coarse mode. Inclusion of nitrate photolysis improves the comparison with fine mode nitrate and leads to a distinct diurnal profile in pNO_3^- which decreases around midday and steadily increases overnight (Figure 2c). As sea salt nitrate makes up >90% of the nitrate at Cabo Verde in the model, mostly in the coarse mode, the pNO_3^- diurnal simulated here is a result of photolysis depleting nitrate aerosol. There appear to be no marine coarse mode nitrate observations at a high enough time resolution available to evaluate this result.

https://doi.org/10.5194/egusphere-2025-830
Preprint. Discussion started: 26 February 2025

Figure 2(d-f) compares the simulations of HONO "background" air (selected as described in Methods Section) with observations from FIREX-AQ, ARNA and the CVAO. Observed HONO mixing ratios across the 3 datasets range between 1 to 100 pptv. Without nitrate photolysis, simulated mixing ratios are substantially lower (<1 pptv) than observations. The inclusion of the Shah parameterization decreases the bias by increasing HONO concentrations at the CVAO (NMB improves from -95% to -16%), with only a minor change for the airborne ARNA (-97% to -95%) and FIREX-AQ (-92% to -81%) campaigns. Inclusion of the new nitrate parameterization increases peak daytime HONO concentrations to >4 ppt for all campaigns, in better agreement with observations. It does however lead to a mean nighttime overestimate of 1.5 ppt (Figure 2f). This is potentially due to dry deposition of HONO in the model being too slow, resulting in higher overnight concentrations than in observations (Yu et al., 2022).

While the inclusion of nitrate photolysis increases HONO concentrations, there remains a daytime underestimate of HONO relative to each of these datasets. This is likely due to the model being biased low for total nitrate concentrations, and thus the model HONO production being too low. To test this hypothesis, we further evaluated the HONO in the FIREX-AQ dataset, subsampling the entire dataset when the model shows various degrees of underestimate in pNO_3^- (Figure 4). When sampling the entire FIREX-AQ dataset, the new parameterization reduced the model HONO underestimate by around a quarter (-85% to -62%). When ignoring data points where the simultaneous pNO_3^- measurement had a low bias of >75%, the HONO bias of the new simulation improved to -30%, while the bias in the Base and Shah simulations showed only very minor changes. The best agreement (NMB of -20%) was found with the new parameterization when only considering data with a pNO_3^- underestimate of less than 25%. This demonstrates that the new parameterization is capable of reproducing measured HONO concentrations reasonably accurately when modelled pNO_3^- is close to observations and that the main limiting factor for the model simulation of HONO is the pNO_3^- bias. It was not possible to replicate this analysis for the ARNA and CVAO datasets due to the amount of data available.

https://doi.org/10.5194/egusphere-2025-830
Preprint. Discussion started: 26 February 2025

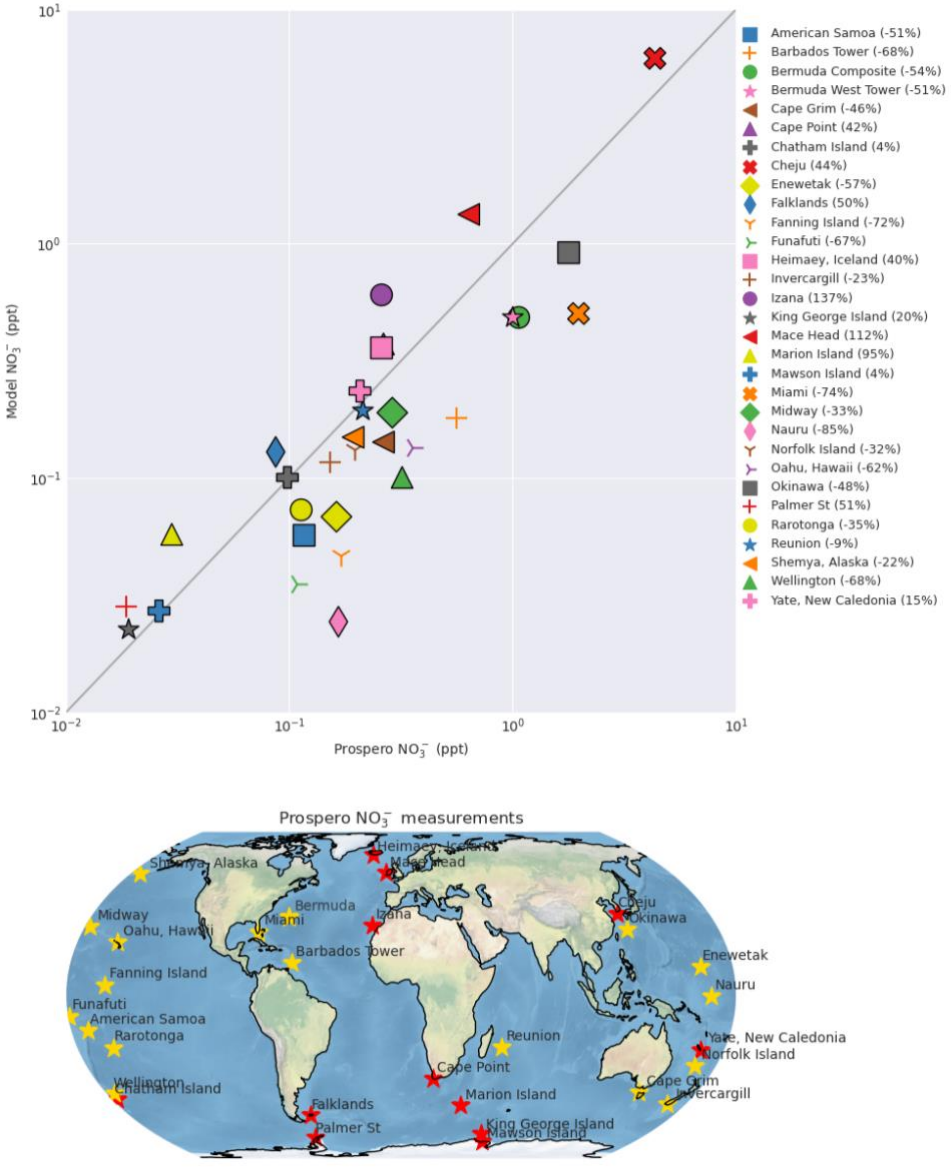

Figure 3. Comparison of total nitrate (pNO_3^-) measurements from the Prospero network (Prospero et al., 2001) with simulated nitrate in the base model simulation. Lower panel shows the locations of the sites. Colour of the marker on the map indicates whether the model overestimates observation (red star) or underestimates (yellow).

The modelled HONO is also compared to measurements from independent datasets SEANA (ship), CAFE (aircraft) and Tudor Hill (in-situ) (see Methods Section) (Figure 5). Across all three datasets the base model has a large underestimate (-89%), which is somewhat reduced by the Shah parameterization (-84%) with further improvement from the new parameterization (-78%), but there remains a large low model bias for HONO. The comparison between the model and the CAFE-Africa campaign is very consistent with the ARNA comparison shown in Figure 2, as these campaigns took place in a similar area of the Atlantic Ocean. Importantly, Figures 2 and 5 demonstrate the persistence of marine background HONO, and highlight the model failure to reproduce these observations without nitrate photolysis or with previous

https://doi.org/10.5194/egusphere-2025-830
Preprint. Discussion started: 26 February 2025

parameterizations. The introduction of a rapid nitrate photolysis parameterization leads to improvements in the simulation, however the model and measurements of HONO cannot be reconciled without substantial improvement in the simulation of total nitrate aerosol in the model (as demonstrated in Figure 4).

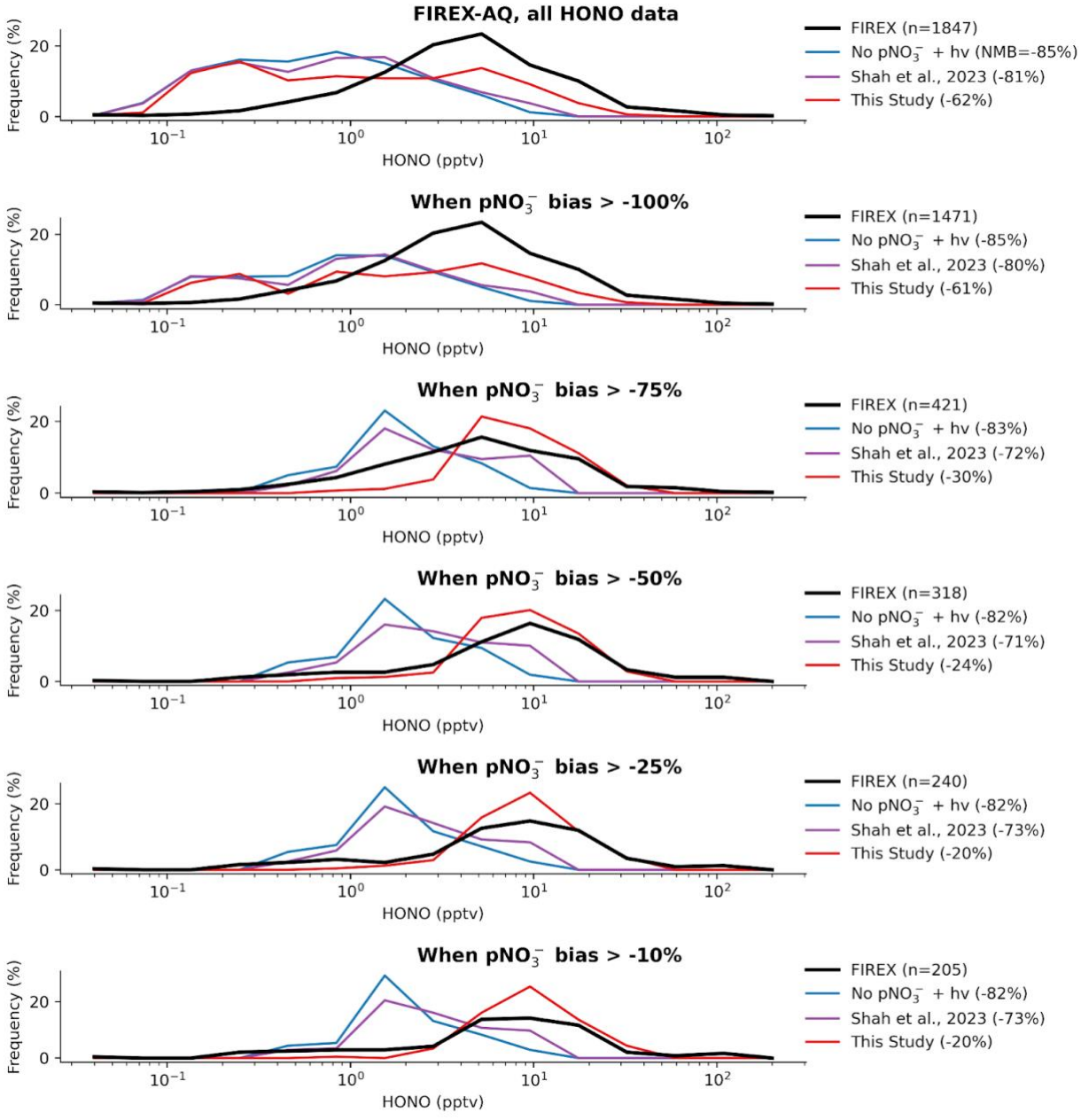

Figure 4. HONO from the FIREX-AQ campaign (black line) compared with simulated HONO for all data (top panel) and with the data filtered by various degrees of pNO_3^- error (lower panels). Number of data points after filtering is shown in the legend of each panel, as well as the NMB of each model simulation.

https://doi.org/10.5194/egusphere-2025-830
Preprint. Discussion started: 26 February 2025

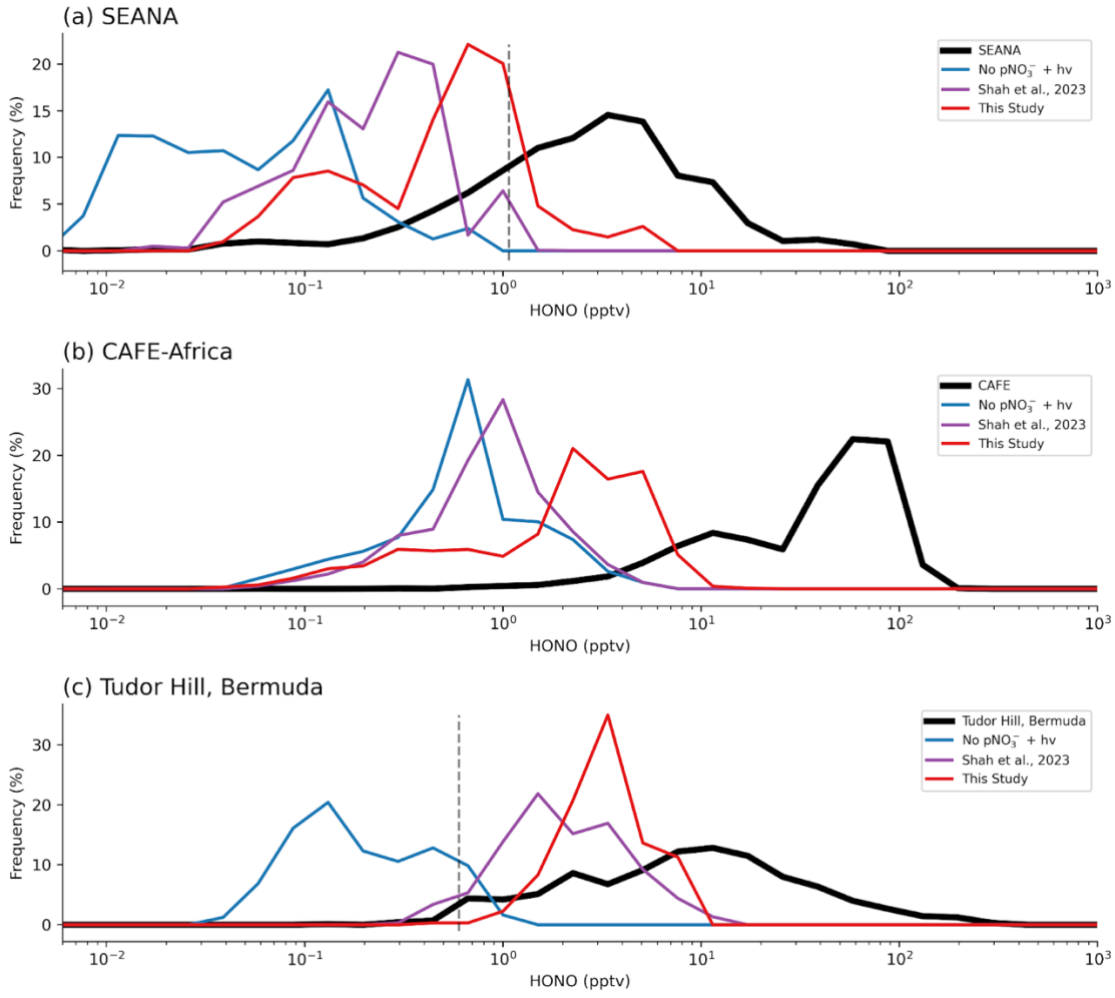

Figure 5. Frequency density comparisons between observed and simulated HONO concentrations during the (a) SEANA ship campaign (surface), (b) CAFE-Africa aircraft campaign (surface to 15km) and (c) in-situ measurements from Tudor Hill, Bermuda (surface) (Zhu et al., 2022). Dashed grey lines represent the estimated limit of detection.

5 Impact on key atmospheric species

The model simulations with and without nitrate photolysis are compared to observed mean vertical profiles from the four NASA ATom missions in Figure 6 (Wofsy et al., 2018). Without nitrate aerosol photolysis, fine mode nitrate aerosol is substantially overestimated by the model (NMB=271%), consistent with Gao et al., 2022. Introducing nitrate photolysis at the rate suggested by Shah does not substantially change the model fine mode nitrate simulation (NMB=243%). However, introducing nitrate photolysis at the rate determined by equation 1 decreases fine mode nitrate, bringing it into better agreement with the observations (NMB=93%), particularly at 2-7km (NMB=20%). The absence of a rapid nitrate photolysis parameterization may thus in part explain the persistent overestimate in fine-mode nitrate described by previous studies (Walker et al., 2012; Miao et al., 2020; Zhai et al., 2021a, 2021b; Gao et al., 2022).

https://doi.org/10.5194/egusphere-2025-830
Preprint. Discussion started: 26 February 2025

All three simulations overestimate the measured HNO_3 from the surface up to 6 km, before largely underestimating above 7 km. Observed values are just 4 ppt at the surface, compared with 24 ppt in the base simulation, 32 ppt with Shah and 37 ppt with the new parameterization. Throughout the ATom profile the base simulation had the lowest NMB of 137%, while the Shah run had the largest at 161%. The new simulation had a NMB of 158%, closer to the measured values in the mid-troposphere than the other simulations (5-7 km, NMB=3%), but with a larger underestimate in the upper troposphere (NMB=33%).

HONO measurements were not made during ATom. Without nitrate photolysis, modeled HONO concentrations are very low (< 0.1 ppt). The Shah parameterization increases concentrations roughly 10-fold in the marine boundary layer with surface concentrations reaching 0.5 ppt. Smaller increases are produced in the free troposphere (50-100%). The new parameterization results in larger increases at the surface (20-fold increase) and has a larger impact through the free troposphere (2-5-fold increase). As a result, the average surface concentrations of HONO are generally > 1 ppt, above the typical instrument detection limit. Future measurements of HONO from airborne campaigns able to span a wide geographic range throughout the marine troposphere would be invaluable to further constrain the current uncertainties.

Without nitrate photolysis, the simulated NO_x is higher than observations at the surface (15 ppt vs 8 ppt measured), roughly consistent with the observations in the boundary layer and lower troposphere (NMB below 6 km = 3%), and lower than observations in the free troposphere (NMB above 6 km = 35%). The Shah parameterization, which was specifically derived to improve the model agreement with NO from ATom, unsurprisingly leads to good agreement throughout the profile (NMB = 7%), albeit with an overestimate at the surface (30 ppt). The new parameterization leads to a large overestimate at the surface (45 ppt) and throughout the vertical profile, more than doubling concentrations (NMB=108%) and pushing concentrations beyond the observational variability.

O_3 and OH concentrations during ATom are relatively well simulated in both the base and Shah simulations. Using the new parameterization leads to a large increase in both O_3 and OH (30% and 53%, respectively), again bringing their concentrations higher than the upper limits of observations.

https://doi.org/10.5194/egusphere-2025-830
Preprint. Discussion started: 26 February 2025

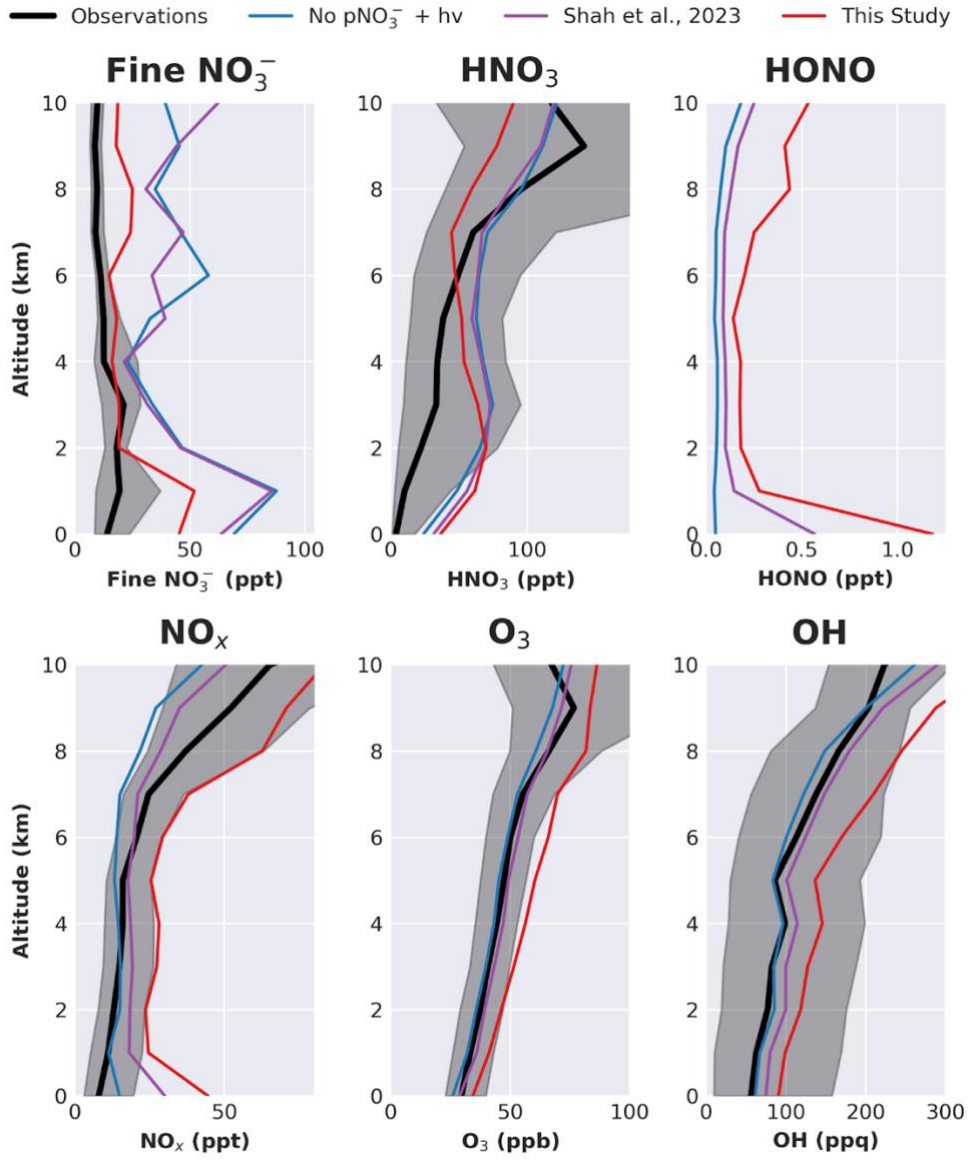

475 **Figure 6.** Median vertical profiles of key species from the ATom campaign (black, shaded area shows 25th-75th percentiles) and in GEOS-Chem simulations co-located with the measurements.

6 Global Atmospheric Impacts

Annual mean tropospheric OH is 1.11×10^6 molec cm^{-3} in the base simulation, well within the range indicated by previous modeling studies of 0.94-1.44 (Zhao et al., 2019; Saunois et al., 2020), but higher than the 1.00×10^6 molec cm^{-3} indicated by
480 recent studies based on methyl chloroform observations (Zhou et al., 2023). Mean simulated tropospheric OH concentrations increase to 1.23 and 1.41 $\times 10^6$ molec cm^{-3} in the Shah and new parameterization simulations, respectively (Table 1). The

https://doi.org/10.5194/egusphere-2025-830
Preprint. Discussion started: 26 February 2025

model OH is at the upper limit of the range from previous studies with the faster parameterization, and substantially higher than the values suggested by observations. The NH:SH OH ratio (Table 2) is overestimated by all three simulations during the ATom campaign, with the overestimate increasing with the introduction of nitrate photolysis and the associated increase in OH concentration. On a global scale, the model still overestimates the NH:SH ratio relative to observational estimates (Bousquet et al., 2005; Patra et al., 2014), although there remains large uncertainty on such estimates (Murray et al., 2013), but is in reasonable agreement with similar modeling studies (Zhou et al., 2023). Nitrate concentrations are higher in the NH primarily due to the distribution of anthropogenic emissions, meaning that the modeled impact of nitrate photolysis is also greater in the NH. As a result, the introduction of nitrate photolysis to the model exacerbates the existing overestimation in NH [OH], pushing the NH:SH ratio further from parity to 1.40 in our parameterization.

Table 1. Summary of key model diagnostics in the 3 GEOS-Chem simulations (percentage change from first simulation is in brackets).

Tropospheric	No pNO_3^- + hv	Shah et al. 2023	This study
OH ($\times 10^6$ molec cm^{-3})	1.11	1.23 (+11%)	1.41 (+27%)
CH_4 lifetime (years)	9.65	8.54 (-12%)	7.50 (-22%)
NO_x burden (Tg)	0.36	0.40 (+11%)	0.52 (+44%)
CO burden (Tg)	326	306 (-6%)	271 (-17%)
O_3 burden (Tg)	319	342 (+7%)	393 (+23%)
O_3 radiative forcing (Wm^{-2})	0.43	0.49 (+14%)	0.69 (+60%)

Table 2. Annual mean tropospheric OH in GEOS-Chem simulations and previous literature, globally and for the ATom campaign (2016-2018).

	OH			
	Global	NH	SH	NH / SH
ATom ($\times 10^{-4}$ ppq)				
Observations	1.8	2.1	1.4	1.48
No pNO_3^- + hv	1.5	2.1	1.3	1.61
Shah et l. 2023	1.7	2.4	1.4	1.72
This Study	3.4	3.3	1.6	2.05
Global ($\times 10^6$ molec cm^{-3})				
Observations[1,2]	0.93-1.12			0.97 ± 0.12
Modelling studies[3,4]	0.93-1.44			
No pNO_3^- + hv	1.11	1.23	0.99	1.24
Shah et l. 2023	1.23	1.38	1.07	1.29
This Study	1.41	1.65	1.18	1.40

[1]Patra et al., 2014; [2]Cressot et al., 2014; [3]Naik et al., 2013; Zhao et al., 2023

https://doi.org/10.5194/egusphere-2025-830
Preprint. Discussion started: 26 February 2025

Figure 7 shows the impact of the new parameterization on global annual mean surface concentrations of HONO, NO_x and O_3. Figure 8 shows the equivalent zonal mean plots. Surface HONO concentrations increase globally when the new nitrate photolysis parameterization is switched on, with maximum increases in mean surface concentrations of ~4-6 ppt found over Asia. Absolute increases are generally higher in the populated NH areas and relative changes are larger over clean regions such as the Southern Ocean and tropical Atlantic / Pacific. Figure 9 shows the same as Figure 7 but for HNO_3, pNO_3^- and OH. As expected, surface pNO_3^- broadly decreases in remote regions, while HNO_3 and OH increase substantially.

For NO_x, the changes vary considerably between continental and ocean regions. The largest absolute changes are in industrialized, polluted regions (Eastern China, Eastern USA, Europe), where surface NO_x decreases by up to 1 ppb (~20%), due to an increase in the NO_2 to NO ratio as a result of the increased O_3 concentrations. This leads to a decrease in the lifetime of NO_x leading to decreased surface concentrations. Over the marine surface, NO_x increases by a factor of 2-4, particularly in the southern hemisphere. Polluted regions already have high levels of NO_x, meaning that the added NO_x from renoxification is relatively less important than in clean, low-NO_x environments. High NO_x concentrations also result in loss of O_3 through titration, limiting the impact in polluted areas (Monks et al., 2015).

The change in surface O_3 is more spatially homogeneous due to its longer lifetime. Relative to the simulation without nitrate photolysis, our parameterization increases annual mean global surface O_3 concentrations by 66%. By comparison, the Shah parameterization increases surface O_3 by 33%. The largest changes are in the NH due to the greater concentration of nitrate. The troposphere in general is NO_x-limited for O_3 production (Sillman et al., 2002; Ivatt et al., 2022), therefore the recycling of reactive nitrogen through nitrate photolysis leads to a near-ubiquitous increase in O_3 production. The greatest absolute increases of ~20 ppb are over NH continental regions and the highest relative increases occur over the tropical and subtropical oceans, where surface O_3 increases by up to 75%, reaching close to 40 ppb in the mid-Pacific. Ozone mixing ratios over the tropical Pacific increase by up to 12 ppb (67%). In populated and polluted regions, the changes tend to be significantly smaller, with increases of ~6 ppb (14%) and 9 ppb (20%) over Eastern China and Western Europe, respectively. A further comparison of O_3 with data from GAW sites (Figure S3) demonstrates the large increase in O_3 in the simulation with the new parameterization, leading to a model overestimate at almost all sites. These analyses demonstrate that while the new parameterization may improve model performance for fine-mode nitrate aerosol and HONO relative to observations, it leads to a substantial inconsistency with observations for NO_x, O_3 and OH.

https://doi.org/10.5194/egusphere-2025-830
Preprint. Discussion started: 26 February 2025

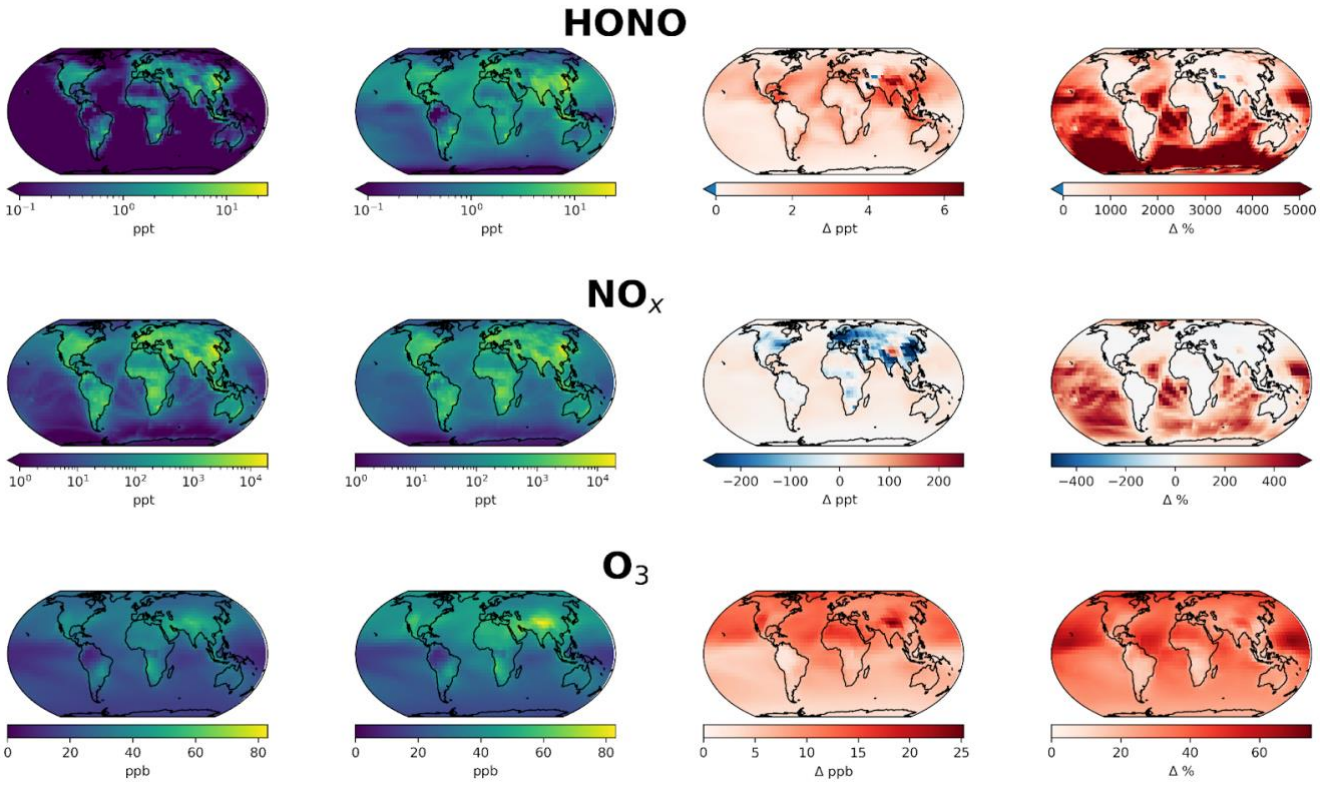

Figure 7. Annual mean surface concentrations of HONO, NO_x ($NO+NO_2$) and O_3 in model simulations (first column) without nitrate photolysis and (second column) with nitrate photolysis as parameterized by equation 1. Absolute difference is shown in the third column and % change in the fourth column.

https://doi.org/10.5194/egusphere-2025-830
Preprint. Discussion started: 26 February 2025

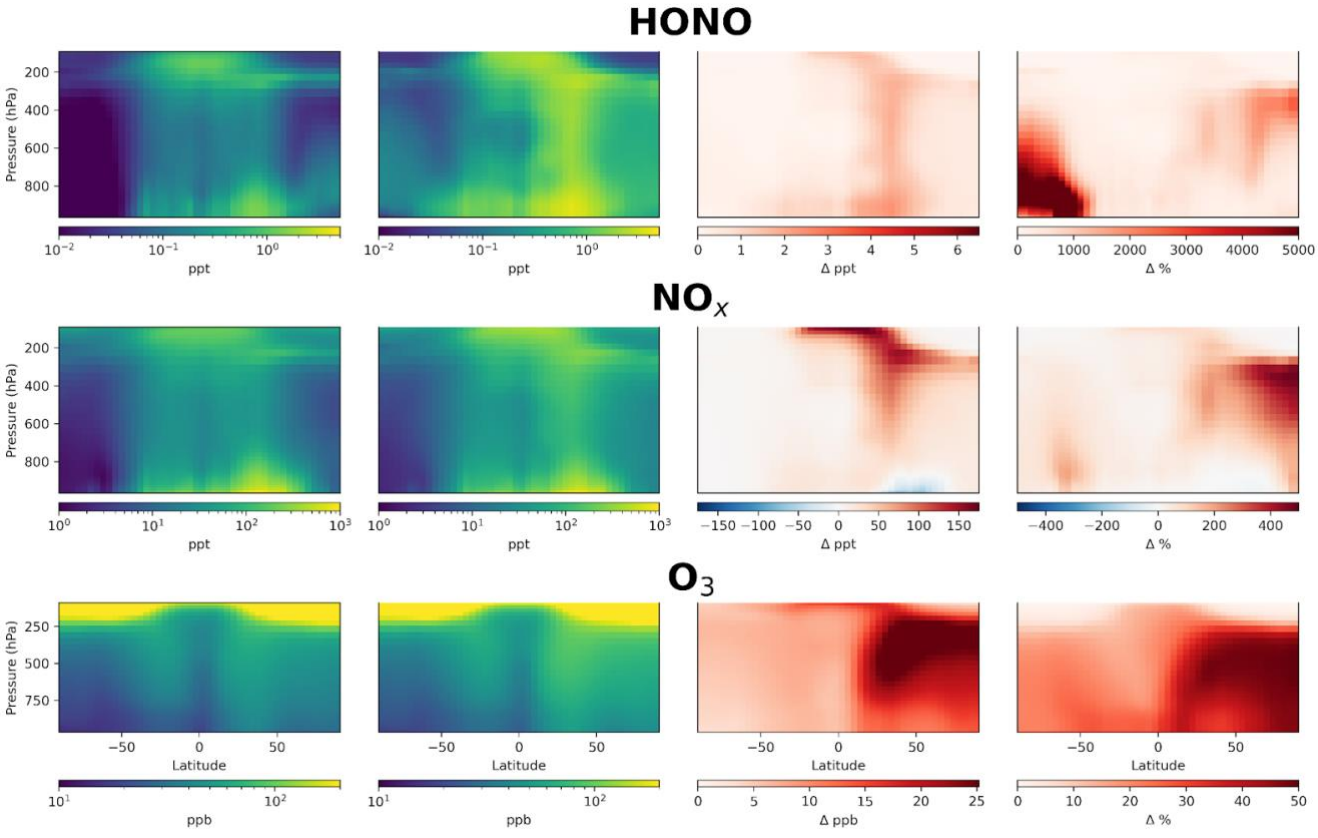

Figure 8. Annual mean zonal concentrations of HONO, NO_x and O_3 in model simulation with (first column) and without (second column) aerosol nitrate photolysis as parameterized by equation 1. Absolute difference is shown in the third column and % change in the fourth column.

https://doi.org/10.5194/egusphere-2025-830
Preprint. Discussion started: 26 February 2025

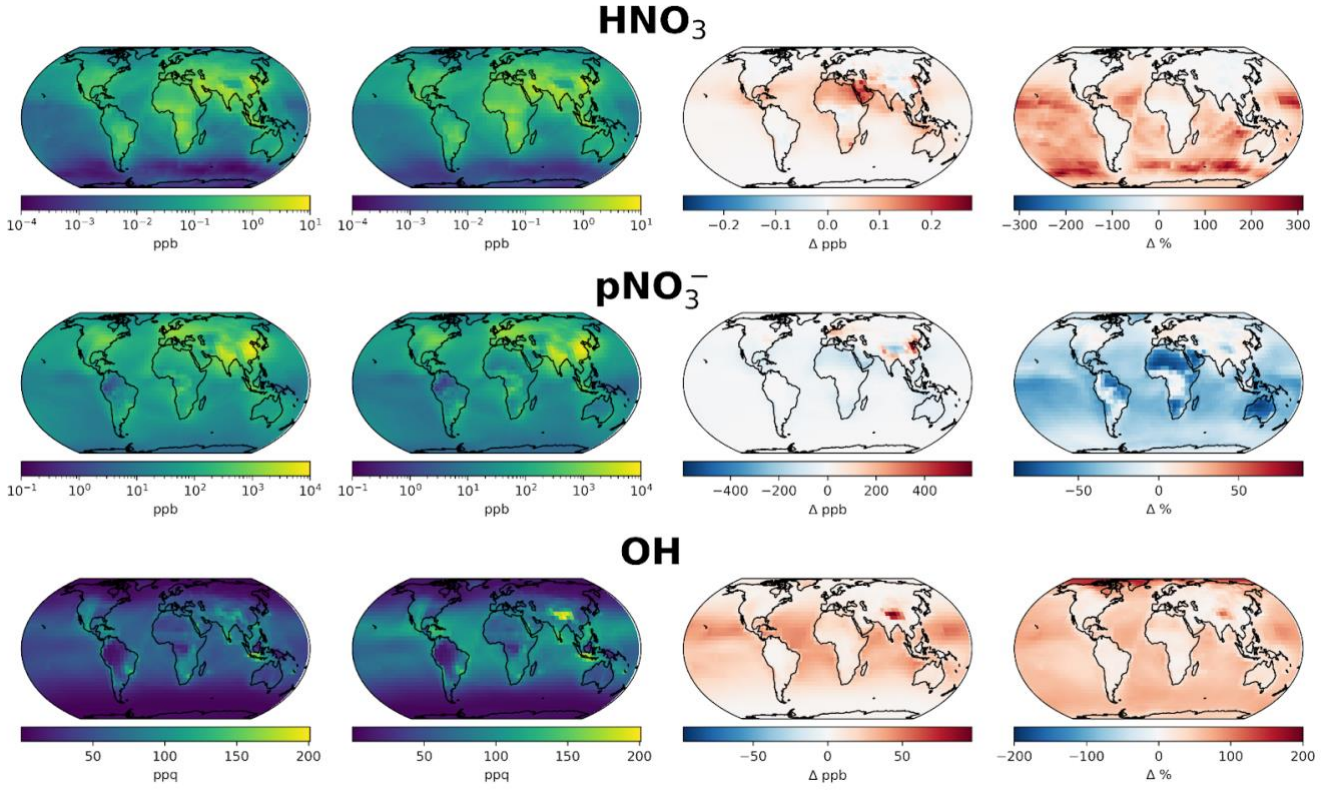

Figure 9. Annual mean surface concentrations of HNO_3, particulate nitrate (pNO_3^-) and OH in model simulation with (first column) and without (second column) aerosol nitrate photolysis as parameterized by equation 1. Absolute difference is shown in the third column and % change in the fourth column.

7 Discussion

The large increase in O_3 following the implementation of our new parameterization has a significant effect on the preindustrial (PI) to present day (PD) tropospheric O_3 radiative forcing (RF) (see Methods section and Table 1). The RF due to O_3 in both the base simulation and that using Shah et al.'s parameterization falls within the expected range from previous modelling studies (0.2-0.6 Wm^{-2}, Myhre et al., 2013), with a 14% increase in RF in the Shah simulation. When using the new parameterization introduced here, the RF due to O_3 increases 60% from the base model to 0.69 Wm^{-2}, outside of the range from previous modelling studies. There are large uncertainties associated with the nitrate aerosol in the preindustrial era, for which there is a lack of solid evidence to evaluate the preindustrial concentrations.

The new parameterization of nitrate photolysis developed here causes substantial changes in the chemical budgets of reactive nitrogen. NO_x is emitted into the atmosphere by anthropogenic combustion processes, biomass burning, lightning and soils, with a total source estimated at ~55 TgN yr^{-1} dominated by anthropogenic combustion of ~31 TgN yr^{-1} (Hoesly et al., 2018; McDuffie et al., 2020; Bray et al., 2021). A simplified schematic of the budget for each simulation is shown in S8-10, while Table S1 summaries the key terms. The most important change in the budget caused by fast nitrate photolysis is the recycling of nitrogen from stable species (pNO_3^-) back into reactive nitrogen (NO_x). Using our new parameterization, this results in an annual NO_x source almost as large as the total global emission of NO_x (48 TgN yr^{-1} compared with 55 TgN

https://doi.org/10.5194/egusphere-2025-830
Preprint. Discussion started: 26 February 2025

yr^{-1}) and larger than the anthropogenic (31 TgN yr^{-1}) (Table S1). Unsurprisingly, this large renoxification term has profound implications for atmospheric chemistry, increasing NO_x concentrations globally, as well as tropospheric O_3 production and OH concentrations. The simulated concentrations of O_3 and OH cannot be reconciled with observations (Figures 6, S3). However, our parameterization still underestimates HONO primarily due to the model underestimate of nitrate aerosol concentrations, as discussed above.

The conclusions made here for the chemistry of the atmosphere are significant, thus it is judicious to explore alternative explanations for these findings. Our analyses are dependent on accurate measurements of HONO concentrations in the remote atmosphere. We utilized data from three different techniques and from four independent research groups (see Methods Section) from remote regions where HONO concentrations were above the limit of detection (~1 pptv) to provide robust observations. We note however that HONO observations are often below the limit of detection of current instrumentation; improved technologies would help to provide greater confidence in the lowest concentrations reported. The renoxification mechanism used to simulate the field observations of HONO shown here is supported by various laboratory estimates of the rate of nitrate photolysis, many of which derive EFs far exceeding those implemented here (Ye et al., 2016; Ye et al., 2017). We note however that even if the nitrate photolysis as applied through this parameterization was overestimated, the observations show that the HONO is significantly higher than the model can reproduce with traditional chemistry. Observations and theory could potentially be reconciled without renoxification if the HONO lifetime (predominantly determined by photolysis) is significantly longer than currently thought. An order of magnitude decrease in the photolysis rate of HONO could essentially remove the disagreement. However, the current photolysis parameters for HONO photolysis (Atkinson et al., 2004) is based on 6 previous studies (Stockwell and Calvert, 1978; Vasudev, 1990; Bongartz et al., 1991; Bongartz et al., 1994; Pagsberg et al., 1997; Wang and Zhang, 2000; Stutz et al., 2000) which agree to within ~15%. Therefore, it is unlikely that the lifetime of HONO is an order of magnitude slower than currently considered, leaving it necessary for other parts of the chemical system to change to remove the inconsistency between HONO observations and observations of O_3, NO_x, OH etc.

There are a number of mechanisms which may decrease NO_x in the atmosphere and thus could go some way to reconciling this discrepancy, by either decreasing the primary NO_x source or by increasing the NO_x sink. Several significant emission sources of NO_x are highly uncertain, including lightning (2-8 Tg yr^{-1}; Murray et al., 2016; Verma et al., 2021), soil (8.5-15 TgN yr^{-1}; Hudman et al., 2012; Vinken et al., 2014; Weng et al., 2020) and biomass burning (11-17 Tg yr^{-1}; Bray et al., 2021). Butkovskaya et al. (2005) observed in laboratory studies a HNO_3-forming branch of the NO + HO_2 reaction, which reduces NOx concentrations by ~20%, and resulted in a mean global OH decrease of 13% and a 5-12% decrease in tropospheric O_3 (Cariolle et al., 2008). Tropospheric halogen chemistry is also uncertain and may contribute to a larger sink for NO_x and O_3 than currently estimated by the model (Iglesias-Suarez et al., 2020; Badia et al., 2021; Wang et al., 2021; Alexander et al., 2020). Stratospheric-tropospheric exchange of O_3 is yet another factor with a large uncertainty, which could account for some of the additional tropospheric O_3 loss required to accommodate the increase due to nitrate photolysis (Wang and Fu, 2021; Ruiz and Prather, 2022). New observations of water vapor absorption in the ultraviolet suggest a reduction in photolysis rates that leads to a global tropospheric OH decrease of ~4% (Prather et al., 2024). Many of these terms result in small and highly uncertain changes in the NO_x, OH and tropospheric O_3, but together may accommodate the large changes that have resulted from improving modelled HONO relative to measurements and demonstrate a general need for improved understanding of tropospheric chemical processes. The implication of these results is that our current understanding of the atmospheric chemistry of NO_x and reactive nitrogen species is incomplete and needs to be improved if we are to have faith in our ability to predict the future chemical state of the atmosphere.

Acknowledgments

This work was supported by the National Environmental Research Council (NERC) grant NE/S000518/1 to L.J.C., M.J.E. and J.D.L. The Cabo Verde Atmospheric Observatory is funded through the National Centre for Atmospheric Science (NCAS). L.J.C. acknowledges funding from the European Research Council (ERC) under the European Union's Horizon 2020 programme (project O3-SML; grant agreement no. 833290). The Viking cluster was used during this project, which is

https://doi.org/10.5194/egusphere-2025-830
Preprint. Discussion started: 26 February 2025

a high-performance compute facility provided by the University of York. We are grateful for computational support from the University of York, IT Services and the Research IT team.

We are grateful for the funding of the HALO aircraft and in particular to the contributions of the German Research Foundation (DFG; HALO-SPP 1294) to the various HALO missions and for the research grants (DFG; grant nos. PF-384/7-1, PF384/9-1, PF-384/16-1, PF-384/17, PF-384/19, PF 384/24-1, and BU 2599/10-1) in support of our measurements from the HALO aircraft.

We acknowledge funding from UK Natural Environment Research Council for the DY151 cruise under the following grants: NE/S00579X/1 (PI Zongbo Shi), NE/S005587/1 (PI Anna Jones), and NE/T00648X/1 (PI Ben Murray). We wish to thank the captain Antione Gatti and the crew of the RRS Discovery, and the National Marine Facility (NMF) team, including NMF technicians (Jon Short, Jack Arnott and Nick Harker) for their support before, during and after the DY151 cruise. We also thank all the science team for their help, discussions and cooperation throughout the campaign.

The CU-Boulder group acknowledges funding from NASA grants 80NSSC21K1451 and 80NSSC23K0828.

The authors would like to thank Glenn Diskin for providing CO measurements used for filtering the FIREX-AQ dataset. We also thank Jack Dibb for providing the FIREX-AQ aerosol filter measurements as well as valuable editorial comments and feedback on the manuscript.

https://doi.org/10.5194/egusphere-2025-830
Preprint. Discussion started: 26 February 2025

References

Alexander, B., Sherwen, T., Holmes, C. D., Fisher, J. A., Chen, Q., Evans, M. J., and Kasibhatla, P.: Global inorganic nitrate production mechanisms: comparison of a global model with nitrate isotope observations, Atmospheric Chemistry and Physics, 20, 3859–3877, https://doi.org/10.5194/acp-20-3859-2020, 2020.

Andersen, S. T., Carpenter, L. J., Reed, C., Lee, J. D., Chance, R., Sherwen, T., Vaughan, A. R., Stewart, J., Edwards, P. M., Bloss, W. J., Sommariva, R., Crilley, L. R., Nott, G. J., Neves, L., Read, K., Heard, D. E., Seakins, P. W., Whalley, L. K., Boustead, G. A., Fleming, L. T., Stone, D., and Fomba, K. W.: Extensive field evidence for the release of HONO from the photolysis of nitrate aerosols, Science Advances, 9, eadd6266, https://doi.org/10.1126/sciadv.add6266, 2023.

Atkinson, R., Baulch, D. L., Cox, R. A., Crowley, J. N., Hampson, R. F., Hynes, R. G., Jenkin, M. E., Rossi, M. J., and Troe, J.: Evaluated kinetic and photochemical data for atmospheric chemistry: Volume I - gas phase reactions of Ox, HOx, NOx and SOx species, Atmospheric Chemistry and Physics, 4, 1461–1738, https://doi.org/10.5194/acp-4-1461-2004, 2004.

Badia, A., Iglesias-Suarez, F., Fernandez, R. P., Cuevas, C. A., Kinnison, D. E., Lamarque, J.-F., Griffiths, P. T., Tarasick, D. W., Liu, J., and Saiz-Lopez, A.: The Role of Natural Halogens in Global Tropospheric Ozone Chemistry and Budget Under Different 21st Century Climate Scenarios, Journal of Geophysical Research: Atmospheres, 126, e2021JD034859, https://doi.org/https://doi.org/10.1029/2021JD034859, e2021JD034859 2021JD034859, 2021.

Bao, F., Jiang, H., Zhang, Y., Li, M., Ye, C., Wang, W., Ge, M., Chen, C., and Zhao, J.: The Key Role of Sulfate in the Photochemical Renoxification on Real PM2.5, Environmental Science & Technology, 54, 3121–3128, https://doi.org/10.1021/acs.est.9b06764, pMID: 32084312, 2020.

Bates, K. H., Jacob, D. J., Li, K., Ivatt, P. D., Evans, M. J., Yan, Y., and Lin, J.: Development and evaluation of a new compact mechanism for aromatic oxidation in atmospheric models, Atmospheric Chemistry and Physics, 21, 18351–18374, https://doi.org/10.5194/acp-2118351-2021, 2021.

Bauer, S. E., Koch, D., Unger, N., Metzger, S. M., Shindell, D. T., and Streets, D. G.: Nitrate aerosols today and in 2030: a global simulation including aerosols and tropospheric ozone, Atmospheric Chemistry and Physics, 7, 5043–5059, https://doi.org/10.5194/acp-7-5043-2007, 2007.

Bauer, S. E., Tsigaridis, K., Faluvegi, G., Kelley, M., Lo, K. K., Miller, R. L., Nazarenko, L., Schmidt, G. A., and Wu, J.: Historical (1850–2014) Aerosol Evolution and Role on Climate Forcing Using the GISS ModelE2.1 Contribution to CMIP6, Journal of Advances in Modeling Earth Systems, 12, e2019MS001978, https://doi.org/https://doi.org/10.1029/2019MS001978, e2019MS001978 2019MS001978, 2020.

Bekki, S.: On the possible role of aircraft-generated soot in the middle latitude ozone depletion, Journal of Geophysical Research: Atmospheres, 102, 10751–10758, https://doi.org/https://doi.org/10.1029/97JD00134, 1997.

Bey, I., Jacob, D. J., Yantosca, R. M., Logan, J. A., Field, B. D., Fiore, A. M., Li, Q., Liu, H. Y., Mickley, L. J., and Schultz, M. G.: Global modeling of tropospheric chemistry with assimilated meteorology: Model description and evaluation, Journal of Geophysical Research: Atmospheres, 106, 23073–23095, https://doi.org/https://doi.org/10.1029/2001JD000807, 2001.

Bongartz, A., Kames, J., Welter, F., and Schurath, U.: Near-UV absorption cross sections and trans/cis equilibrium of nitrous acid, The Journal of Physical Chemistry, 95, 1076–1082, https://doi.org/10.1021/j100156a012, 1991.

Bongartz, A., Kames, J., Schurath, U., George, C., Mirabel, P., and Ponche, J. L.: Experimental determination of HONO mass accommodation coefficients using two different techniques, Journal of Atmospheric Chemistry, 18, 149–169, https://doi.org/10.1007/BF00696812, 1994.

https://doi.org/10.5194/egusphere-2025-830
Preprint. Discussion started: 26 February 2025

Bourgeois, I., Peischl, J., Neuman, J. A., Brown, S. S., Allen, H. M., Campuzano-Jost, P., Coggon, M. M., DiGangi, J. P., Diskin, G. S., Gilman, J. B., Gkatzelis, G. I., Guo, H., Halliday, H. A., Hanisco, T. F., Holmes, C. D., Huey, L. G., Jimenez, J. L., Lamplugh, A. D., Lee, Y. R., Lindaas, J., Moore, R. H., Nault, B. A., Nowak, J. B., Pagonis, D., Rickly, P. S., Robinson, M. A., Rollins, A. W., Selimovic, V., St. Clair, J. M., Tanner, D., Vasquez, K. T., Veres, P. R., Warneke, C., Wennberg, P. O., Washenfelder, R. A., Wiggins, E. B., Womack, C. C., Xu, L., Zarzana, K. J., and Ryerson, T. B.: Comparison of airborne measurements of NO, NO_2, HONO, NO_y, and CO during FIREX-AQ, Atmospheric Measurement Techniques, 15, 4901–4930, https://doi.org/10.5194/amt-15-4901-2022, 2022.

Bousquet, P., Hauglustaine, D. A., Peylin, P., Carouge, C., and Ciais, P.: Two decades of OH variability as inferred by an inversion of atmospheric transport and chemistry of methyl chloroform, Atmospheric Chemistry and Physics, 5, 2635–2656, https://doi.org/10.5194/acp-52635-2005, 2005.

Bray, C. D., Battye, W. H., Aneja, V. P., and Schlesinger, W. H.: Global emissions of NH3, NOx, and N2O from biomass burning and the impact of climate change, Journal of the Air & Waste Management Association, 71, 102–114, https://doi.org/10.1080/10962247.2020.1842822, pMID: 33125305, 2021.

Butkovskaya, N. I., Kukui, A., Pouvesle, N., and Le Bras, G.: Formation of Nitric Acid in the Gas-Phase HO2 + NO Reaction: Effects of Temperature and Water Vapor, The Journal of Physical Chemistry A, 109, 6509–6520, https://doi.org/10.1021/jp051534v, pMID: 16833996, 2005.

Cariolle, D., Evans, M. J., Chipperfield, M. P., Butkovskaya, N., Kukui, A., and Le Bras, G.: Impact of the new HNO_3-forming channel of the HO_2+NO reaction on tropospheric HNO_3, NO_x, HO_x and ozone, Atmospheric Chemistry and Physics, 8, 4061–4068, https://doi.org/10.5194/acp-8-4061-2008, 2008.

Carpenter, L. J., Fleming, Z. L., Read, K. A., Lee, J. D., Moller, S. J., Hopkins, J. R., Purvis, R. M., Lewis, A. C., Moller, K., Heinold, B., Herrmann, H., Fomba, K. W., van Pinxteren, D., M√ºller, C., Tegen, I., Wiedensohler, A., M√ºller, T., Niedermeier, N., Achterberg, E. P., Patey, M. D., Kozlova, E. A., Heimann, M., Heard, D. E., Plane, J. M. C., Mahajan, A., Oetjen, H., Ingham, T., Stone, D., Whalley, L. K., Evans, M. J., Pilling, M. J., Leigh, R. J., Monks, P. S., Karunaharan, A., Vaughan, S., Arnold, S. R., Tschritter, J., P√∂hler, D., Frie√ü, U., Holla, R., Mendes, L. M., Lopez, H., Faria, B., Manning, A. J., and Wallace, D. W. R.: Seasonal characteristics of tropical marine boundary layer air measured at the Cape Verde Atmospheric Observatory, Journal of Atmospheric Chemistry, 67, 87–140, https://doi.org/10.1007/s10874-011-9206-1, 2010.

Crilley, L. R., Kramer, L. J., Pope, F. D., Reed, C., Lee, J. D., Carpenter, L. J., Hollis, L. D. J., Ball, S. M., and Bloss, W. J.: Is the ocean surface a source of nitrous acid (HONO) in the marine boundary layer?, Atmospheric Chemistry and Physics, 21, 18213–18225, https://doi.org/10.5194/acp-21-18213-2021, 2021.

Dibb, J. E., Jaffrezo, J. L., and Bergin, M. H.: ATM aerosol concentrations around the GISP ice core site, https://doi.org/10.1594/PANGAEA.56077, 1999.

Dibb, J. E., Talbot, R. W., Seid, G., Jordan, C., Scheuer, E., Atlas, E., Blake, N. J., and Blake, D. R.: Airborne sampling of aerosol particles: Comparison between surface sampling at Christmas Island and P-3 sampling during PEM-Tropics B, Journal of Geophysical Research: Atmospheres, 107, PEM 2–1–PEM 2–17, https://doi.org/https://doi.org/10.1029/2001JD000408, 2002.

Du, J. and Zhu, L.: Quantification of the absorption cross sections of surface-adsorbed nitric acid in the 335–365nm region by Brewster angle cavity ring-down spectroscopy, Chemical Physics Letters, 511, 213–218, https://doi.org/https://doi.org/10.1016/j.cplett.2011.06.062, 2011.

Fomba, K. W., Müller, K., van Pinxteren, D., Poulain, L., van Pinxteren, M., and Herrmann, H.: Long-term chemical characterization of tropical and marine aerosols at the Cape Verde Atmospheric Observatory (CVAO) from 2007 to 2011, Atmospheric Chemistry and Physics, 14, 8883–8904, https://doi.org/10.5194/acp-14-8883-2014, 2014.

https://doi.org/10.5194/egusphere-2025-830
Preprint. Discussion started: 26 February 2025

Gao, C. Y., Heald, C. L., Katich, J. M., Luo, G., and Yu, F.: Remote Aerosol Simulated During the Atmospheric Tomography (ATom) Campaign and Implications for Aerosol Lifetime, Journal of Geophysical Research: Atmospheres, 127, e2022JD036524, https://doi.org/https://doi.org/10.1029/2022JD036524, e2022JD036524 2022JD036524, 2022.

Gaudel, A., Cooper, O. R., Ancellet, G., Barret, B., Boynard, A., Burrows, J. P., Clerbaux, C., Coheur, P.-F., Cuesta, J., Cuevas, E., Doniki, S., Dufour, G., Ebojie, F., Foret, G., Garcia, O., Granados-Muñoz, M. J., Hannigan, J. W., Hase, F., Hassler, B., Huang, G., Hurtmans, D., Jaffe, D., Jones, N., Kalabokas, P., Kerridge, B., Kulawik, S., Latter, B., Leblanc, T., Le Flochmoën, E., Lin, W., Liu, J., Liu, X., Mahieu, E., McClure-Begley, A., Neu, J. L., Osman, M., Palm, M., Petetin, H., Petropavlovskikh, I., Querel, R., Rahpoe, N., Rozanov, A., Schultz, M. G., Schwab, J., Siddans, R., Smale, D., Steinbacher, M., Tanimoto, H., Tarasick, D. W., Thouret, V., Thompson, A. M., Trickl, T., Weatherhead, E., Wespes, C., Worden, H. M., Vigouroux, C., Xu, X., Zeng, G., and Ziemke, J.: Tropospheric Ozone Assessment Report: Present-day distribution and trends of tropospheric ozone relevant to climate and global atmospheric chemistry model evaluation, Elementa: Science of the Anthropocene, 6, 39, https://doi.org/10.1525/elementa.291, 2018.

Gelaro, R., McCarty, W., Suárez, M. J., Todling, R., Molod, A., Takacs, L., Randles, C. A., Darmenov, A., Bosilovich, M. G., Reichle, R., Wargan, K., Coy, L., Cullather, R., Draper, C., Akella, S., Buchard, V., Conaty, A., da Silva, A. M., Gu, W., Kim, G.-K., Koster, R., Lucchesi, R., Merkova, D., Nielsen, J. E., Partyka, G., Pawson, S., Putman, W., Rienecker, M., Schubert, S. D., Sienkiewicz, M., and Zhao, B.: The Modern-Era Retrospective Analysis for Research and Applications, Version 2 (MERRA-2), Journal of Climate, 30, 5419 – 5454, https://doi.org/10.1175/JCLI-D-16-0758.1, 2017.

Gen, M., Liang, Z., Zhang, R., Go, B. R., and Chan, C. K.: Particulate nitrate photolysis in the atmosphere, Environ. Sci.: Atmos., 2, 111–127, https://doi.org/10.1039/D1EA00087J, 2022.

Glowacki, D. R., Goddard, A., Hemavibool, K., Malkin, T. L., Commane, R., Anderson, F., Bloss, W. J., Heard, D. E., Ingham, T., Pilling, M. J., and Seakins, P. W.: Design of and initial results from a Highly Instrumented Reactor for Atmospheric Chemistry (HIRAC), Atmospheric Chemistry and Physics, 7, 5371–5390, https://doi.org/10.5194/acp-7-5371-2007, 2007.

Guenther, A., Hewitt, C. N., Erickson, D., Fall, R., Geron, C., Graedel, T., Harley, P., Klinger, L., Lerdau, M., Mckay, W. A., Pierce, T., Scholes, B., Steinbrecher, R., Tallamraju, R., Taylor, J., and Zimmerman, P.: A global model of natural volatile organic compound emissions, Journal of Geophysical Research: Atmospheres, 100, 8873–8892, https://doi.org/https://doi.org/10.1029/94JD02950, 1995.

Guo, H., Campuzano-Jost, P., Nault, B. A., Day, D. A., Schroder, J. C., Kim, D., Dibb, J. E., Dollner, M., Weinzierl, B., and Jimenez, J. L.: The importance of size ranges in aerosol instrument intercomparisons: a case study for the Atmospheric Tomography Mission, Atmospheric Measurement Techniques, 14, 3631–3655, https://doi.org/10.5194/amt-14-3631-2021, 2021.

Heland, J., Kleffmann, J., Kurtenbach, R., and Wiesen, P.: A New Instrument To Measure Gaseous Nitrous Acid (HONO) in the Atmosphere, Environmental Science & Technology, 35, 3207–3212, https://doi.org/10.1021/es000303t, pMID: 11506004, 2001.

Hoesly, R. M., Smith, S. J., Feng, L., Klimont, Z., Janssens-Maenhout, G., Pitkanen, T., Seibert, J. J., Vu, L., Andres, R. J., Bolt, R. M., Bond, T. C., Dawidowski, L., Kholod, N., Kurokawa, J.-I., Li, M., Liu, L., Lu, Z., Moura, M. C. P., O'Rourke, P. R., and Zhang, Q.: Historical (1750–2014) anthropogenic emissions of reactive gases and aerosols from the Community Emissions Data System (CEDS), Geoscientific Model Development, 11, 369–408, https://doi.org/10.5194/gmd-11-369-2018, 2018.

Hua, W., Verreault, D., and Allen, H. C.: Surface Electric Fields of Aqueous Solutions of NH4NO3, Mg(NO3)2, NaNO3, and LiNO3: Implications for Atmospheric Aerosol Chemistry, The Journal of Physical Chemistry C, 118, 24941–24949, https://doi.org/10.1021/jp505770t, 2014.

Hudman, R. C., Moore, N. E., Mebust, A. K., Martin, R. V., Russell, A. R., Valin, L. C., and Cohen, R. C.: Steps towards a mechanistic model of global soil nitric oxide emissions: implementation and space based-constraints, Atmospheric Chemistry and Physics, 12, 7779–7795, https://doi.org/10.5194/acp-12-7779-2012, 2012.

Iglesias-Suarez, F., Badia, A., Fernandez, R. P., Cuevas, C. A., Kinnison, D. E., Tilmes, S., Lamarque, J.-F., Long, M. C., Hossaini, R., and Saiz-Lopez, A.: Natural halogens buffer tropospheric ozone in a changing climate, Nature Climate Change, 10, 147–154, https://doi.org/10.1038/s41558-019-0675-6, 2020.

Ivatt, P. D., Evans, M. J., and Lewis, A. C.: Suppression of surface ozone by an aerosol-inhibited photochemical ozone regime, Nature Geoscience, 15, 536–540, https://doi.org/10.1038/s41561-022-00972-9, 2022.

Jiang, Y., Xia, M., Xue, L., Wang, X., Zhong, X., Liu, Y., Kulmala, M., Ma, T., Wang, J., Wang, Y., Gao, J., and Wang, T.: Quantifying HONO Production from Nitrate Photolysis in a Polluted Atmosphere, Environmental Science & Technology, 58, 14361–14371, https://doi.org/10.1021/acs.est.4c06061, pMID: 39088841, 2024.

Kasibhatla, P., Sherwen, T., Evans, M. J., Carpenter, L. J., Reed, C., Alexander, B., Chen, Q., Sulprizio, M. P., Lee, J. D., Read, K. A., Bloss, W., Crilley, L. R., Keene, W. C., Pszenny, A. A. P., and Hodzic, A.: Global impact of nitrate photolysis in sea-salt aerosol on NO_x, OH, and O_3 in the marine boundary layer, Atmospheric Chemistry and Physics, 18, 11185–11203, https://doi.org/10.5194/acp-18-11185-2018, 2018.

Kleffmann, J.: Daytime Sources of Nitrous Acid (HONO) in the Atmospheric Boundary Layer, ChemPhysChem, 8, 1137–1144, https://doi.org/https://doi.org/10.1002/cphc.200700016, 2007.

Kleffmann, J. and Wiesen, P.: Technical Note: Quantification of interferences of wet chemical HONO LOPAP measurements under simulated polar conditions, Atmospheric Chemistry and Physics, 8, 6813–6822, https://doi.org/10.5194/acp-8-6813-2008, 2008.

Knipping, E. M. and Dabdub, D.: Modeling surface-mediated renoxification of the atmosphere via reaction of gaseous nitric oxide with deposited nitric acid, Atmospheric Environment, 36, 5741–5748, https://doi.org/https://doi.org/10.1016/S1352-2310(02)00652-0, 2002.

Lary, D. J., Lee, A. M., Toumi, R., Newchurch, M. J., Pirre, M., and Renard, J. B.: Carbon aerosols and atmospheric photochemistry, Journal of Geophysical Research: Atmospheres, 102, 3671–3682, https://doi.org/https://doi.org/10.1029/96JD02969, 1997.

Lee, B. H., Lopez-Hilfiker, F. D., Mohr, C., Kurtén, T., Worsnop, D. R., and Thornton, J. A.: An Iodide-Adduct High-Resolution Time-ofFlight Chemical-Ionization Mass Spectrometer: Application to Atmospheric Inorganic and Organic Compounds, Environmental Science & Technology, 48, 6309–6317, https://doi.org/10.1021/es500362a, pMID: 24800638, 2014.

Li, B., Gao, J., Chen, C., Wen, L., Zhang, Y., Li, J., Zhang, Y., Du, X., Zhang, K., and Wang, J.: Exploring HONO production from particulate nitrate photolysis in representative regions of China: characteristics, influencing factors, and environmental implications, Atmospheric Chemistry and Physics, 24, 13183–13198, https://doi.org/10.5194/acp-24-13183-2024, 2024.

McDuffie, E. E., Smith, S. J., O'Rourke, P., Tibrewal, K., Venkataraman, C., Marais, E. A., Zheng, B., Crippa, M., Brauer, M., and Martin, R. V.: A global anthropogenic emission inventory of atmospheric pollutants from sector- and fuel-specific sources (1970–2017): an application of the Community Emissions Data System (CEDS), Earth System Science Data, 12, 3413–3442, https://doi.org/10.5194/essd12-3413-2020, 2020.

Meinshausen, M., Vogel, E., Nauels, A., Lorbacher, K., Meinshausen, N., Etheridge, D. M., Fraser, P. J., Montzka, S. A., Rayner, P. J., Trudinger, C. M., Krummel, P. B., Beyerle, U., Canadell, J. G., Daniel, J. S., Enting, I. G., Law, R. M., Lunder, C. R., O'Doherty, S., Prinn, R. G., Reimann, S., Rubino, M., Velders, G. J. M., Vollmer, M. K., Wang, R. H. J., and Weiss,

R.: Historical greenhouse gas concentrations for climate modelling (CMIP6), Geoscientific Model Development, 10, 2057–2116, https://doi.org/10.5194/gmd-10-2057-2017, 2017.

Meng, Z., Dabdub, D., and Seinfeld, J. H.: Chemical Coupling Between Atmospheric Ozone and Particulate Matter, Science, 277, 116–119, https://doi.org/10.1126/science.277.5322.116, 1997.

Miao, R., Chen, Q., Zheng, Y., Cheng, X., Sun, Y., Palmer, P. I., Shrivastava, M., Guo, J., Zhang, Q., Liu, Y., Tan, Z., Ma, X., Chen, S., Zeng, L., Lu, K., and Zhang, Y.: Model bias in simulating major chemical components of $PM_{2.5}$ in China, Atmospheric Chemistry and Physics, 20, 12265–12284, https://doi.org/10.5194/acp-20-12265-2020, 2020.

Monks, P. S., Archibald, A. T., Colette, A., Cooper, O., Coyle, M., Derwent, R., Fowler, D., Granier, C., Law, K. S., Mills, G. E., Stevenson, D. S., Tarasova, O., Thouret, V., von Schneidemesser, E., Sommariva, R., Wild, O., and Williams, M. L.: Tropospheric ozone and its precursors from the urban to the global scale from air quality to short-lived climate forcer, Atmospheric Chemistry and Physics, 15, 8889–8973, https://doi.org/10.5194/acp-15-8889-2015, 2015.

Murray, L. T.: Lightning NOxand Impacts on Air Quality, Current Pollution Reports, 2, 115–133, https://doi.org/10.1007/s40726-016-00317, 2016.

Murray, L. T., Logan, J. A., and Jacob, D. J.: Interannual variability in tropical tropospheric ozone and OH: The role of lightning, Journal of Geophysical Research: Atmospheres, 118, 11,468–11,480, https://doi.org/https://doi.org/10.1002/jgrd.50857, 2013.

Myhre, G., Shindell, D., Bréon, F.-M., Collins, W., Fuglestvedt, J., Huang, J., Koch, D., Lamarque, J.-F., Lee, D., Mendoza, B., Nakajima, T., Robock, A., Stephens, G., Takemura, T., and Zhang, H.: Anthropogenic and natural radiative forcing, pp. 659–740, Cambridge University Press, Cambridge, UK, https://doi.org/10.1017/CBO9781107415324.018, 2013.

Nault, B. A., Campuzano-Jost, P., Day, Douglas A.and Jo, D. S., Schroder, J. C., Allen, H. M., Bahreini, R., Bian, H., Blake, D. R., Chin, M., Clegg, S. L., Colarco, P. R., Crounse, J. D., Cubison, M. J., DeCarlo, P. F., Dibb, J. E., Diskin, G. S., Hodzic, A., Hu, W., Katich, J. M., Kim, M. J., Kodros, J. K., Kupc, A., Lopez-Hilfiker, F. D., Marais, E. A., Middlebrook, A. M., Andrew Neuman, J., Nowak, J. B., Palm, B. B., Paulot, F., Pierce, J. R., Schill, Gregory P.and Scheuer, E., Thornton, J. A., Tsigaridis, K., Wennberg, P. O., Williamson, C. J., and Jimenez, J. L.: Chemical transport models often underestimate inorganic aerosol acidity in remote regions of the atmosphere, Communications Earth & Environment, 2, 93, https://doi.org/10.1038/s43247-021-00164-0, 2021.

Ndour, M., Conchon, P., D'Anna, B., Ka, O., and George, C.: Photochemistry of mineral dust surface as a potential atmospheric renoxification process, Geophysical Research Letters, 36, https://doi.org/https://doi.org/10.1029/2008GL036662, 2009.

Nguyen, D.-H., Lin, C., Vu, C.-T., Cheruiyot, N. K., Nguyen, M. K., Le, T. H., Lukkhasorn, W., Vo, T.-D.-H., and Bui, X.-T.: Tropospheric ozone and NOx: A review of worldwide variation and meteorological influences, Environmental Technology and Innovation, 28, 102809, https://doi.org/https://doi.org/10.1016/j.eti.2022.102809, 2022.

Ninneman, M., Lu, S., Zhou, X., and Schwab, J.: On the Importance of Surface-Enhanced Renoxification as an Oxides of Nitrogen Source in Rural and Urban New York State, ACS Earth and Space Chemistry, 4, 1985–1992, https://doi.org/10.1021/acsearthspacechem.0c00185, 2020.

Pagsberg, P., Bjergbakke, E., Ratajczak, E., and Sillesen, A.: Kinetics of the gas phase reaction OH + NO(+M)−→HONO(+M) and the determination of the UV absorption cross sections of HONO, Chemical Physics Letters, 272, 383–390, https://doi.org/https://doi.org/10.1016/S0009-2614(97)00576-9, 1997.

https://doi.org/10.5194/egusphere-2025-830
Preprint. Discussion started: 26 February 2025

Parrish, D. D., Norton, R. B., Bollinger, M. J., Liu, S. C., Murphy, P. C., Albritton, D. L., Fehsenfeld, F. C., and Huebert, B. J.: Measurements of HNO3 and NO3 - particulates at a rural site in the Colorado mountains, Journal of Geophysical Research: Atmospheres, 91, 5379–5393, https://doi.org/https://doi.org/10.1029/JD091iD05p05379, 1986.

Patra, P. K., Krol, M. C., Montzka, S. A., Arnold, T., Atlas, E. L., Lintner, B. R., Stephens, B. B., Xiang, B., Elkins, J. W., Fraser, P. J., Ghosh, A., Hintsa, E. J., Hurst, D. F., Ishijima, K., Krummel, P. B., Miller, B. R., Miyazaki, K., Moore, F. L., M√ºhle, J., O,ÄôDoherty, S., Prinn, R. G., Steele, L. P., Takigawa, M., Wang, H. J., Weiss, R. F., Wofsy, S. C., and Young, D.: Observational evidence for interhemispheric hydroxyl-radical parity, Nature, 513, 219–223, https://doi.org/10.1038/nature13721, 2014.

Prather, M. J. and Zhu, L.: Resetting tropospheric OH and CH₄ lifetime with ultraviolet H₂O absorption, Science, 385, 201–204, https://doi.org/10.1126/science.adn0415, 2024.

Ramazan, K. A., Wingen, L. M., Miller, Y., Chaban, G. M., Gerber, R. B., Xantheas, S. S., and Finlayson-Pitts, B. J.: New Experimental and Theoretical Approach to the Heterogeneous Hydrolysis of NO2: Key Role of Molecular Nitric Acid and Its Complexes, The Journal of Physical Chemistry A, 110, 6886–6897, https://doi.org/10.1021/jp056426n, pMID: 16722704, 2006.

Reed, C., Brumby, C. A., Crilley, L. R., Kramer, L. J., Bloss, W. J., Seakins, P. W., Lee, J. D., and Carpenter, L. J.: HONO measurement by differential photolysis, Atmospheric Measurement Techniques, 9, 2483–2495, https://doi.org/10.5194/amt-9-2483-2016, 2016.

Reed, C., Evans, M. J., Crilley, L. R., Bloss, W. J., Sherwen, T., Read, K. A., Lee, J. D., and Carpenter, L. J.: Evidence for renoxification in the tropical marine boundary layer, Atmospheric Chemistry and Physics, 17, 4081–4092, https://doi.org/10.5194/acp-17-4081-2017, 2017.

Richards, N. K. and Finlayson-Pitts, B. J.: Production of Gas Phase NO2 and Halogens from the Photochemical Oxidation of Aqueous Mixtures of Sea Salt and Nitrate Ions at Room Temperature, Environmental Science & Technology, 46, 10447–10454, https://doi.org/10.1021/es300607c, pMID: 22506935, 2012.

Ruiz, D. J. and Prather, M. J.: From the middle stratosphere to the surface, using nitrous oxide to constrain the stratosphere–troposphere exchange of ozone, Atmospheric Chemistry and Physics, 22, 2079–2093, https://doi.org/10.5194/acp-22-2079-2022, 2022.

Sachse, G. W., Hill, G. F., Wade, L. O., and Perry, M. G.: Fast-response, high-precision carbon monoxide sensor using a tunable diode laser absorption technique, Journal of Geophysical Research: Atmospheres, 92, 2071–2081, https://doi.org/https://doi.org/10.1029/JD092iD02p02071, 1987.

Sachse, G. W., Jr., J. E. C., Hill, G. F., Wade, L. O., Burney, L. G., and Ritter, J. A.: Airborne tunable diode laser sensor for high-precision concentration and flux measurements of carbon monoxide and methane, in: Measurement of Atmospheric Gases, edited by Schiff, H. I., vol. 1433, pp. 157 – 166, International Society for Optics and Photonics, SPIE, https://doi.org/10.1117/12.46162, 1991.

Saunois, M., Stavert, A. R., Poulter, B., Bousquet, P., Canadell, J. G., Jackson, R. B., Raymond, P. A., Dlugokencky, E. J., Houweling, S., Patra, P. K., Ciais, P., Arora, V. K., Bastviken, D., Bergamaschi, P., Blake, D. R., Brailsford, G., Bruhwiler, L., Carlson, K. M., Carrol, M., Castaldi, S., Chandra, N., Crevoisier, C., Crill, P. M., Covey, K., Curry, C. L., Etiope, G., Frankenberg, C., Gedney, N., Hegglin, M. I., Höglund-Isaksson, L., Hugelius, G., Ishizawa, M., Ito, A., Janssens-Maenhout, G., Jensen, K. M., Joos, F., Kleinen, T., Krummel, P. B., Langenfelds, R. L., Laruelle, G. G., Liu, L., Machida, T., Maksyutov, S., McDonald, K. C., McNorton, J., Miller, P. A., Melton, J. R., Morino, I., Müller, J., Murguia-Flores, F., Naik, V., Niwa, Y., Noce, S., O'Doherty, S., Parker, R. J., Peng, C., Peng, S., Peters, G. P., Prigent, C., Prinn, R., Ramonet, M., Regnier, P., Riley, W. J., Rosentreter, J. A., Segers, A., Simpson, I. J., Shi, H., Smith, S. J., Steele, L. P., Thornton, B. F., Tian, H., Tohjima, Y., Tubiello, F. N., Tsuruta, A., Viovy, N., Voulgarakis, A., Weber, T. S., van Weele, M., van der Werf, G. R., Weiss, R. F.,

https://doi.org/10.5194/egusphere-2025-830
Preprint. Discussion started: 26 February 2025

Worthy, D., Wunch, D., Yin, Y., Yoshida, Y., Zhang, W., Zhang, Z., Zhao, Y., Zheng, B., Zhu, Q., Zhu, Q., and Zhuang, Q.: The Global Methane Budget 2000–2017, Earth System Science Data, 12, 1561–1623, https://doi.org/10.5194/essd-12-1561-2020, 2020.

Scheuer, E., Talbot, R. W., Dibb, J. E., Seid, G. K., DeBell, L., and Lefer, B.: Seasonal distributions of fine aerosol sulfate in the North American Arctic basin during TOPSE, Journal of Geophysical Research: Atmospheres, 108, https://doi.org/https://doi.org/10.1029/2001JD001364, 2003.

Shah, V., Jacob, D. J., Dang, R., Lamsal, L. N., Strode, S. A., Steenrod, S. D., Boersma, K. F., Eastham, S. D., Fritz, T. M., Thompson, C., Peischl, J., Bourgeois, I., Pollack, I. B., Nault, B. A., Cohen, R. C., Campuzano-Jost, P., Jimenez, J. L., Andersen, S. T., Carpenter, L. J., Sherwen, T., and Evans, M. J.: Nitrogen oxides in the free troposphere: implications for tropospheric oxidants and the interpretation of satellite NO_2 measurements, Atmospheric Chemistry and Physics, 23, 1227–1257, https://doi.org/10.5194/acp-23-1227-2023, 2023.

Shah, V., Keller, C. A., Knowland, K. E., Christiansen, A., Hu, L., Wang, H., Lu, X., Alexander, B., and Jacob, D. J.: Particulate Nitrate Photolysis as a Possible Driver of Rising Tropospheric Ozone, Geophysical Research Letters, 51, e2023GL107980, https://doi.org/https://doi.org/10.1029/2023GL107980, e2023GL107980 2023GL107980, 2024.

Shi, Q., Tao, Y., Krechmer, J. E., Heald, C. L., Murphy, J. G., Kroll, J. H., and Ye, Q.: Laboratory Investigation of Renoxification from the Photolysis of Inorganic Particulate Nitrate, Environmental Science & Technology, 55, 854–861, https://doi.org/10.1021/acs.est.0c06049, pMID: 33393757, 2021.

Sillman, S. and He, D.: Some theoretical results concerning O3-NO-VOC chemistry and NO-VOC indicators, Journal of Geophysical Research: Atmospheres, 107, ACH 26–1–ACH 26–15, https://doi.org/https://doi.org/10.1029/2001JD001123, 2002.

Sommariva, R., Alam, M. S., Crilley, L. R., Rooney, D. J., Bloss, W. J., Fomba, K. W., Andersen, S. T., and Carpenter, L. J.: Factors Influencing the Formation of Nitrous Acid from Photolysis of Particulate Nitrate, The Journal of Physical Chemistry A, 127, 9302–9310, https://doi.org/10.1021/acs.jpca.3c03853, pMID: 37879076, 2023.

Song, M., Zhao, X., Liu, P., Mu, J., He, G., Zhang, C., Tong, S., Xue, C., Zhao, X., Ge, M., and Mu, Y.: Atmospheric NOx oxidation as major sources for nitrous acid (HONO), Npj Climate and Atmospheric Science, 6, 30, https://doi.org/10.1038/s41612-023-00357-8, 2023.

Stavrakou, T., Müller, J.-F., Boersma, K. F., van der A, R. J., Kurokawa, J., Ohara, T., and Zhang, Q.: Key chemical NO_x sink uncertainties and how they influence top-down emissions of nitrogen oxides, Atmospheric Chemistry and Physics, 13, 9057–9082, https://doi.org/10.5194/acp-13-9057-2013, 2013.

Stevenson, D. S., Young, P. J., Naik, V., Lamarque, J.-F., Shindell, D. T., Voulgarakis, A., Skeie, R. B., Dalsoren, S. B., Myhre, G., Berntsen, T. K., Folberth, G. A., Rumbold, S. T., Collins, W. J., MacKenzie, I. A., Doherty, R. M., Zeng, G., van Noije, T. P. C., Strunk, A., Bergmann, D., Cameron-Smith, P., Plummer, D. A., Strode, S. A., Horowitz, L., Lee, Y. H., Szopa, S., Sudo, K., Nagashima, T., Josse, B., Cionni, I., Righi, M., Eyring, V., Conley, A., Bowman, K. W., Wild, O., and Archibald, A.: Tropospheric ozone changes, radiative forcing and attribution to emissions in the Atmospheric Chemistry and Climate Model Intercomparison Project (ACCMIP), Atmospheric Chemistry and Physics, 13, 3063–3085, https://doi.org/10.5194/acp-13-3063-2013, 2013.

Stockwell, W. R. and Calvert, J. G.: The near ultraviolet absorption spectrum of gaseous HONO and N2O3, Journal of Photochemistry, 8, 193–203, https://doi.org/https://doi.org/10.1016/0047-2670(78)80019-7, 1978.

Stutz, J., Kim, E. S., Platt, U., Bruno, P., Perrino, C., and Febo, A.: UV-visible absorption cross sections of nitrous acid, Journal of Geophysical Research: Atmospheres, 105, 14 585–14 592, https://doi.org/https://doi.org/10.1029/2000JD900003, 2000.

Szopa, S., Naik, V., Adhikary, B., Artaxo, P., Berntsen, T., Collins, W., Fuzzi, S., Gallardo, L., Kiendler-Scharr, A., Klimont, Z., Liao, H., Unger, N., and Zanis, P.: Short-Lived Climate Forcers. In Climate Change 2021: The Physical Science Basis. Contribution of Working Group I to the Sixth Assessment Report of the Intergovernmental Panel on Climate Change, Report, IPCC, https://doi.org/doi:10.1017/9781009157896.008, 2021.

Thompson, C. R., Wofsy, S. C., Prather, M. J., Newman, P. A., Hanisco, T. F., Ryerson, T. B., Fahey, D. W., Apel, E. C., Brock, C. A., Brune, W. H., Froyd, K., Katich, J. M., Nicely, J. M., Peischl, J., Ray, E., Veres, P. R., Wang, S., Allen, H. M., Asher, E., Bian, H., Blake, D., Bourgeois, I., Budney, J., Bui, T. P., Butler, A., Campuzano-Jost, P., Chang, C., Chin, M., Commane, R., Correa, G., Crounse, J. D., Daube, B., Dibb, J. E., DiGangi, J. P., Diskin, G. S., Dollner, M., Elkins, J. W., Fiore, A. M., Flynn, C. M., Guo, H., Hall, S. R., Hannun, R. A., Hills, A., Hintsa, E. J., Hodzic, A., Hornbrook, R. S., Huey, L. G., Jimenez, J. L., Keeling, R. F., Kim, M. J., Kupc, A., Lacey, F., Lait, L. R., Lamarque, J.-F., Liu, J., McKain, K., Meinardi, S., Miller, D. O., Montzka, S. A., Moore, F. L., Morgan, E. J., Murphy, D. M., Murray, L. T., Nault, B. A., Neuman, J. A., Nguyen, L., Gonzalez, Y., Rollins, A., Rosenlof, K., Sargent, M., Schill, G., Schwarz, J. P., Clair, J. M. S., Steenrod, S. D., Stephens, B. B., Strahan, S. E., Strode, S. A., Sweeney, C., Thames, A. B., Ullmann, K., Wagner, N., Weber, R., Weinzierl, B., Wennberg, P. O., Williamson, C. J., Wolfe, G. M., and Zeng, L.: The NASA Atmospheric Tomography (ATom) Mission: Imaging the Chemistry of the Global Atmosphere, Bulletin of the American Meteorological Society, 103, E761 – E790, https://doi.org/10.1175/BAMS-D-20-0315.1, 2022.

van der Werf, G. R., Randerson, J. T., Giglio, L., van Leeuwen, T. T., Chen, Y., Rogers, B. M., Mu, M., van Marle, M. J. E., Morton, D. C., Collatz, G. J., Yokelson, R. J., and Kasibhatla, P. S.: Global fire emissions estimates during 1997–2016, Earth System Science Data, 9, 697–720, https://doi.org/10.5194/essd-9-697-2017, 2017.

Vasudev, R.: Absorption spectrum and solar photodissociation of gaseous nitrous acid in the actinic - wavelength region, Geophysical Research Letters, 17, 2153–2155, https://doi.org/https://doi.org/10.1029/GL017i012p02153, 1990.

Veres, P. R., Neuman, J. A., Bertram, T. H., Assaf, E., Wolfe, G. M., Williamson, C. J., Weinzierl, B., Tilmes, S., Thompson, C. R., Thames, A. B., Schroder, J. C., Saiz-Lopez, A., Rollins, A. W., Roberts, J. M., Price, D., Peischl, J., Nault, B. A., Møller, K. H., Miller, D. O., Meinardi, S., Li, Q., Lamarque, J.-F., Kupc, A., Kjaergaard, H. G., Kinnison, D., Jimenez, J. L., Jernigan, C. M., Hornbrook, R. S., Hills, A., Dollner, M., Day, D. A., Cuevas, C. A., Campuzano-Jost, P., Burkholder, J., Bui, T. P., Brune, W. H., Brown, S. S., Brock, C. A., Bourgeois, I., Blake, D. R., Apel, E. C., and Ryerson, T. B.: Global airborne sampling reveals a previously unobserved dimethyl sulfide oxidation mechanism in the marine atmosphere, Proceedings of the National Academy of Sciences, 117, 4505–4510, https://doi.org/10.1073/pnas.1919344117, 2020.

Verma, S., Yadava, P. K., Lal, D. M., Mall, R. K., Kumar, H., and Payra, S.: Role of Lightning NOx in Ozone Formation: A Review, Pure and Applied Geophysics, 178, 1425–1443, https://doi.org/10.1007/s00024-021-02710-5, 2021.

Vinken, G. C. M., Boersma, K. F., Maasakkers, J. D., Adon, M., and Martin, R. V.: Worldwide biogenic soil NO_x emissions inferred from OMI NO_2 observations, Atmospheric Chemistry and Physics, 14, 10363–10381, https://doi.org/10.5194/acp-14-10363-2014, 2014.

Virtanen, P., Gommers, R., Oliphant, T. E., Haberland, M., Reddy, T., Cournapeau, D., Burovski, E., Peterson, P., Weckesser, W., Bright, J., van der Walt, S. J., Brett, M., Wilson, J., Millman, K. J., Mayorov, N., Nelson, A. R. J., Jones, E., Kern, R., Larson, E., Carey, C. J., Polat, ˙I., Feng, Y., Moore, E. W., VanderPlas, J., Laxalde, D., Perktold, J., Cimrman, R., Henriksen, I., Quintero, E. A., Harris, C. R., Archibald, A. M., Ribeiro, A. H., Pedregosa, F., van Mulbregt, P., and SciPy 1.0 Contributors: SciPy 1.0: Fundamental Algorithms for Scientific Computing in Python, Nature Methods, 17, 261–272, https://doi.org/10.1038/s41592-019-0686-2, 2020.

Walker, J. M., Philip, S., Martin, R. V., and Seinfeld, J. H.: Simulation of nitrate, sulfate, and ammonium aerosols over the United States, Atmospheric Chemistry and Physics, 12, 11213–11227, https://doi.org/10.5194/acp-12-11213-2012, 2012.

Wang, L. and Zhang, J.: Detection of Nitrous Acid by Cavity Ring-Down Spectroscopy, Environmental Science & Technology, 34, 4221– 4227, https://doi.org/10.1021/es0011055, 2000.

https://doi.org/10.5194/egusphere-2025-830
Preprint. Discussion started: 26 February 2025

Wang, M. and Fu, Q.: Stratosphere-Troposphere Exchange of Air Masses and Ozone Concentrations Based on Reanalyses and Observations, Journal of Geophysical Research: Atmospheres, 126, e2021JD035159, https://doi.org/https://doi.org/10.1029/2021JD035159, e2021JD035159 2021JD035159, 2021.

Wang, X., Jacob, D. J., Downs, W., Zhai, S., Zhu, L., Shah, V., Holmes, C. D., Sherwen, T., Alexander, B., Evans, M. J., Eastham, S. D., Neuman, J. A., Veres, P. R., Koenig, T. K., Volkamer, R., Huey, L. G., Bannan, T. J., Percival, C. J., Lee, B. H., and Thornton, J. A.: Global tropospheric halogen (Cl, Br, I) chemistry and its impact on oxidants, Atmospheric Chemistry and Physics, 21, 13973–13996, https://doi.org/10.5194/acp-21-13973-2021, 2021.

Warneke, C., Schwarz, J. P., Dibb, J., Kalashnikova, O., Frost, G., Al-Saad, J., Brown, S. S., Brewer, W. A., Soja, A., Seidel, F. C., Washenfelder, R. A., Wiggins, E. B., Moore, R. H., Anderson, B. E., Jordan, C., Yacovitch, T. I., Herndon, S. C., Liu, S., Kuwayama, T., Jaffe, D., Johnston, N., Selimovic, V., Yokelson, R., Giles, D. M., Holben, B. N., Goloub, P., Popovici, I., Trainer, M., Kumar, A., Pierce, R. B., Fahey, D., Roberts, J., Gargulinski, E. M., Peterson, D. A., Ye, X., Thapa, L. H., Saide, P. E., Fite, C. H., Holmes, C. D., Wang, S., Coggon, M. M., Decker, Z. C. J., Stockwell, C. E., Xu, L., Gkatzelis, G., Aikin, K., Lefer, B., Kaspari, J., Griffin, D., Zeng, L., Weber, R., Hastings, M., Chai, J., Wolfe, G. M., Hanisco, T. F., Liao, J., Campuzano Jost, P., Guo, H., Jimenez, J. L., Crawford, J., and Team, T. F.-A. S.: Fire Influence on Regional to Global Environments and Air Quality (FIREX-AQ), Journal of Geophysical Research: Atmospheres, 128, e2022JD037758, https://doi.org/https://doi.org/10.1029/2022JD037758, e2022JD037758 2022JD037758, 2023.

Weng, H., Lin, J., Martin, R., Millet, D. B., Jaegl√©, L., Ridley, D., Keller, C., Li, C., Du, M., and Meng, J.: Global high-resolution emissions of soil NOx, sea salt aerosols, and biogenic volatile organic compounds, Scientific Data, 7, 148, https://doi.org/10.1038/s41597-020-04885, 2020.

Weyland, B.: Detection of nitrous acid in the lower, middle, and upper troposphere: potential formation mechanisms of excess HONO, Ph.D. thesis, Combined Faculty of Mathematics, Engineering and Natural Sciences of Heidelberg University, Germany, 2024.

Wingen, L. M., Moskun, A. C., Johnson, S. N., Thomas, J. L., Roeselová, M., Tobias, D. J., Kleinman, M. T., and Finlayson-Pitts, B. J.: Enhanced surface photochemistry in chloride-nitrate ion mixtures, Phys. Chem. Chem. Phys., 10, 5668–5677, 2008.

Wofsy, S., Afshar, S., Allen, H., Apel, E., Asher, E., Barletta, B., Bent, J., Bian, H., Biggs, B., Blake, D., Blake, N., Bourgeois, I., Brock, C., Brune, W., Budney, J., Bui, T., Butler, A., Campuzano-Jost, P., Chang, C., Chin, M., Commane, R., Correa, G., Crounse, J., Cullis, P. D., Daube, B., Day, D., Dean-Day, J., Dibb, J., DiGangi, J., Diskin, G., Dollner, M., Elkins, J., Erdesz, F., Fiore, A., Flynn, C., Froyd, K., Gesler, D., Hall, S., Hanisco, T., Hannun, R., Hills, A., Hintsa, E., Hoffman, A., Hornbrook, R., Huey, L., Hughes, S., Jimenez, J., Johnson, B., Katich, J., Keeling, R., Kim, M., Kupc, A., Lait, L., McKain, K., Mclaughlin, R., Meinardi, S., Miller, D., Montzka, S., Moore, F., Morgan, E., Murphy, D., Murray, L., Nault, B., Neuman, J., Newman, P., Nicely, J., Pan, X., Paplawsky, W., Peischl, J., Prather, M., Price, D., Ray, E., Reeves, J., Richardson, M., Rollins, A., Rosenlof, K., Ryerson, T., Scheuer, E., Schill, G., Schroder, J., Schwarz, J., St.Clair, J., Steenrod, S., Stephens, B., Strode, S., Sweeney, C., Tanner, D., Teng, A., Thames, A., Thompson, C., Ullmann, K., Veres, P., Wagner, N., Watt, A., Weber, R., Weinzierl, B., Wennberg, P., Williamson, C., Wilson, J., Wolfe, G., Woods, C., Zeng, L., and Vieznor, N.: ATom: Merged Atmospheric Chemistry, Trace Gases, and Aerosols, Version 2, https://doi.org/10.3334/ORNLDAAC/1925, 2021.

Ye, C., Zhou, X., Pu, D., Stutz, J., Festa, J., Spolaor, M., Tsai, C., Cantrell, C., Mauldin, R. L., Campos, T., Weinheimer, A., Hornbrook, R. S., Apel, E. C., Guenther, A., Kaser, L., Yuan, B., Karl, T., Haggerty, J., Hall, S., Ullmann, K., Smith, J. N., Ortega, J., and Knote, C.: Rapid cycling of reactive nitrogen in the marine boundary layer, Nature, 532, 489–491, https://doi.org/10.1038/nature17195, 2016.

Ye, C., Zhang, N., Gao, H., and Zhou, X.: Photolysis of Particulate Nitrate as a Source of HONO and NOx, Environmental Science & Technology, 51, 6849–6856, https://doi.org/10.1021/acs.est.7b00387, pMID: 28505434, 2017.

Ye, C., Zhou, X., Zhang, Y., Wang, Y., Wang, J., Zhang, C., Woodward-Massey, R., Cantrell, C., Mauldin, R. L., Campos, T., Hornbrook, R. S., Ortega, J., Apel, E. C., Haggerty, J., Hall, S., Ullmann, K., Weinheimer, A., Stutz, J., Karl, T., Smith, J. N., Guenther, A., and Song, S.: Synthesizing evidence for the external cycling of NOx in high- to low-NOx atmospheres, Nature Communications, 14, 7995, https://doi.org/10.1038/s41467-023-43866-z, 2023.

Yu, Y., Cheng, P., Li, H., Yang, W., Han, B., Song, W., Hu, W., Wang, X., Yuan, B., Shao, M., Huang, Z., Li, Z., Zheng, J., Wang, H., and Yu, X.: Budget of nitrous acid (HONO) at an urban site in the fall season of Guangzhou, China, Atmospheric Chemistry and Physics, 22, 8951–8971, https://doi.org/10.5194/acp-22-8951-2022, 2022.

Zhai, S., Jacob, D. J., Brewer, J. F., Li, K., Moch, J. M., Kim, J., Lee, S., Lim, H., Lee, H. C., Kuk, S. K., Park, R. J., Jeong, J. I., Wang, X., Liu, P., Luo, G., Yu, F., Meng, J., Martin, R. V., Travis, K. R., Hair, J. W., Anderson, B. E., Dibb, J. E., Jimenez, J. L., Campuzano-Jost, P., Nault, B. A., Woo, J.-H., Kim, Y., Zhang, Q., and Liao, H.: Relating geostationary satellite measurements of aerosol optical depth (AOD) over East Asia to fine particulate matter ($PM_{2.5}$): insights from the KORUS-AQ aircraft campaign and GEOS-Chem model simulations, Atmospheric Chemistry and Physics, 21, 16775–16791, https://doi.org/10.5194/acp-21-16775-2021, 2021a.

Zhai, S., Jacob, D. J., Wang, X., Liu, Z., Wen, T., Shah, V., Li, K., Moch, J. M., Bates, K. H., Song, S., Shen, L., Zhang, Y., Luo, G., Yu, F., Sun, Y., Wang, L., Qi, M., Tao, J., Gui, K., Xu, H., Zhang, Q., Zhao, T., Wang, Y., Lee, H. C., Choi, H., and Liao, H.: Control of particulate nitrate air pollution in China, Nature Geoscience, 14, 389–395, https://doi.org/10.1038/s41561-021-00726-z, 2021b.

Zhang, Y., Sun, J., Shen, X., Lal Chandani, V., Du, M., Song, C., Dai, Y., Hu, G., Yang, M., Tilstone, G. H., Jordan, T., Dall'Olmo, G., Liu, Q., Nemitz, E., Callaghan, A., Brean, J., Sommariva, R., Beddows, D., Langford, B., Bloss, W., Acton, W., Harrison, R., Dall'Osto, M., and Shi, Z.: Measurements of particulate methanesulfonic acid above the remote Arctic Ocean using a high resolution aerosol mass spectrometer, Atmospheric Environment, 331, 120538, https://doi.org/https://doi.org/10.1016/j.atmosenv.2024.120538, 2024.

Zhao, Y., Saunois, M., Bousquet, P., Lin, X., Berchet, A., Hegglin, M. I., Canadell, J. G., Jackson, R. B., Hauglustaine, D. A., Szopa, S., Stavert, A. R., Abraham, N. L., Archibald, A. T., Bekki, S., Deushi, M., Jöckel, P., Josse, B., Kinnison, D., Kirner, O., Marécal, V., O'Connor, F. M., Plummer, D. A., Revell, L. E., Rozanov, E., Stenke, A., Strode, S., Tilmes, S., Dlugokencky, E. J., and Zheng, B.: Intermodel comparison of global hydroxyl radical (OH) distributions and their impact on atmospheric methane over the 2000–2016 period, Atmospheric Chemistry and Physics, 19, 13701–13723, https://doi.org/10.5194/acp-19-13701-2019, 2019.

Zhao, Y., Saunois, M., Bousquet, P., Lin, X., Hegglin, M. I., Canadell, J. G., Jackson, R. B., and Zheng, B.: Reconciling the bottom-up and top-down estimates of the methane chemical sink using multiple observations, Atmospheric Chemistry and Physics, 23, 789–807, https://doi.org/10.5194/acp-23-789-2023, 2023.

Zhong, X., Shen, H., Zhao, M., Zhang, J., Sun, Y., Liu, Y., Zhang, Y., Shan, Y., Li, H., Mu, J., Yang, Y., Nie, Y., Tang, J., Dong, C., Wang, X., Zhu, Y., Guo, M., Wang, W., and Xue, L.: Nitrous acid budgets in the coastal atmosphere: potential daytime marine sources, Atmospheric Chemistry and Physics, 23, 14761–14778, https://doi.org/10.5194/acp-23-14761-2023, 2023.

Zhu, C., Xiang, B., Chu, L. T., and Zhu, L.: 308 nm Photolysis of Nitric Acid in the Gas Phase, on Aluminum Surfaces, and on Ice Films, The Journal of Physical Chemistry A, 114, 2561–2568, https://doi.org/10.1021/jp909867a, pMID: 20121260, 2010.

Zhu, Y., Wang, Y., Zhou, X., Elshorbany, Y. F., Ye, C., Hayden, M., and Peters, A. J.: An investigation into the chemistry of HONO in the marine boundary layer at Tudor Hill Marine Atmospheric Observatory in Bermuda, Atmospheric Chemistry and Physics, 22, 6327–6346, https://doi.org/10.5194/acp-22-6327-2022, 2022.